

## **Autophagy maintains stemness by preventing senescence**

Laura García-Prat<sup>1</sup>, Marta Martínez-Vicente<sup>2^</sup>, Eusebio Perdiguero<sup>1</sup>, Laura Ortet<sup>1</sup>, Javier Rodríguez-Ubreva<sup>3</sup>, Elena Rebollo<sup>4</sup>, Vanessa Ruiz-Bonilla<sup>1</sup>, Susana Gutarra<sup>1</sup>, Esteban Ballestar<sup>3</sup>, Antonio L. Serrano<sup>1</sup>, Marco Sandri<sup>5^</sup> and Pura Muñoz-Cánoves<sup>1,6\*</sup>

<sup>1</sup>Cell Biology Group, Department of Experimental and Health Sciences, Pompeu Fabra University (UPF), CIBER on Neurodegenerative diseases (CIBERNED), E-08003 Barcelona, Spain; <sup>2</sup>Neurodegenerative Diseases Research Group, Vall d'Hebron Research Institute-CIBERNED, E-08035 Barcelona, Spain; <sup>3</sup>Chromatin and Disease Group, Cancer Epigenetics and Biology Programme (PEBC), Bellvitge Biomedical Research Institute (IDIBELL), E-08907 L'Hospitalet de Llobregat, Barcelona, Spain; <sup>4</sup>Molecular Biology Institute of Barcelona (IBMB-CSIC), 08028 Barcelona, Spain; <sup>5</sup>Department of Biomedical Science, University of Padova, 35100 Padova, Italy. Telethon Institute of Genetics and Medicine (TIGEM), 80131 Napoli, Italy; <sup>6</sup>ICREA, Barcelona, Spain.

<sup>^</sup>Equal contribution

\*Corresponding author:

Pura Muñoz-Cánoves ([pura.munoz@upf.edu](mailto:pura.munoz@upf.edu))

## **SUMMARY**

During aging, muscle stem cell regenerative function declines. At advanced geriatric age, this decline is maximal due to transition from a normal quiescence into an irreversible senescence state. How satellite cells maintain quiescence and avoid senescence during their long life remains largely unknown. Here we report that basal autophagy is indispensable to maintain the stem-cell quiescent state in mice. Failure of autophagy in physiologically aged satellite cells or its genetic impairment in young cells causes senescence entry by loss of proteostasis, increased mitochondrial dysfunction and oxidative stress, resulting in numerical and functional satellite cell decline. Autophagy reestablishment reverses senescence and restores regenerative functions in geriatric satellite cells. Since autophagy also declines in human geriatric satellite cells, these findings uncover autophagy as a decisive stem cell-fate regulator and have implications for fostering muscle regeneration in sarcopenia.



The regenerative capacity of skeletal muscle relies on long-lived Pax7-expressing muscle stem cells (called satellite cells), which are normally in quiescence (a G0 reversible arrest state). In response to tissue damage, these cells activate, enter the cell cycle and either expand and form new myofibers or self-renew to restore the quiescent satellite cell pool<sup>1-4</sup>. Quiescence therefore appears as a simple way of functionally maintaining the stem cell population throughout life in the absence of regenerative demand, particularly in tissues with little turnover, such as skeletal muscle.

Sarcopenia, the age-related loss of skeletal muscle mass and function, is maximal at geriatric age. At this last stage of life, skeletal muscle shows a profound regenerative impairment that contributes to the individual's physical incapacitation. Recent studies have demonstrated that aged skeletal muscles fail to retain stem cell quiescence<sup>5-7</sup>. Both the number and the functionality of muscle stem cells decline with aging<sup>5-10</sup>, with satellite cells switching from a quiescence to a pre-senescence state in sarcopenic muscle at geriatric age<sup>6</sup>. How satellite cells maintain quiescence during their long life and avoid acquisition of the senescence program until advanced age is largely unknown.

Using physiologically aged mice, we show that quiescent muscle stem cells preserve their integrity over time through active maintenance of organelle and protein homeostasis (proteostasis) as cellular quality control mechanism. In particular, we demonstrate that these dormant stem cells display continuous basal macroautophagy (from now on 'autophagy'; i.e. the process for degradation of long-lived proteins and damaged organelles in lysosomes<sup>11,12</sup>). With aging, this activity declines. Physiological decline of autophagy in old satellite cells, or its genetic impairment in young cells, results in toxic cellular waste accumulation, which provokes senescence entry.

Our results indicate that muscle stem cells preserve their G0-reversible quiescence state from entering a G0-irreversible senescence state through autophagy. Importantly, genetic and pharmacological regimes that reinstall basal autophagy in geriatric mice reversed stem cell senescence and restored regeneration. These findings have implications for regenerative medicine in sarcopenia.

## RESULTS

### Quiescent muscle stem cells basal autophagy is impaired in aging

We interrogated the quiescent satellite cell transcriptome for changes in proteostasis genes (as compared to activated cells)<sup>13-15</sup> and uncovered autophagy as the most prevalent pathway in the quiescent state (Extended Data Fig. 1a; Supplementary Table 1). K-means clustering analysis revealed an age-associated downregulation of autophagic genes in quiescence (Extended Data Fig. 1b; Supplementary Table 1).

Autophagy is an evolutionary conserved process of self-degradation of cellular components (organelles, cytosol portions and misfolded proteins) by autophagosomes which are delivered to the lysosomal machinery, thus preventing waste accumulation<sup>11,12</sup>, and which has been implicated in aging of different model organisms<sup>11,12,16,17</sup>. To investigate the occurrence of autophagy in quiescent muscle stem cells we used GFP-LC3 (a well-known marker of autophagosomes) transgenic mice<sup>18,19</sup>. Quiescent satellite cells were fluorescence-activated cell sorting (FACS)-isolated (Extended Data Fig. 1c) from resting muscle of young (3 months) and old GFP-LC3 mice (20-24 months). Punctate GFP-LC3-staining was found in young cells, being increased in old cells (Fig. 1a; Extended Data Fig. 1d; Supplementary Video 1-2). We next used the autophagy-flux inhibitor Bafilomycin (Baf), that prevents lysosome degradation, thus increasing punctate GFP-LC3 exclusively when autophagy is active<sup>20</sup>, as a proxy for autophagic activity. At variance with young cells, Baf treatment demonstrated the old satellite cells' incapacity for further autophagosome formation, as shown by GFP-LC3 fluorescence levels (Fig. 1b). These results indicate, first, constitutive autophagic activity in young quiescent satellite cells; and, second, impaired activity during aging. Fluorescence, transmission-electron microscopy and Western-blotting analyses confirmed in old satellite cells the accumulation of autophagic vesicles (Extended Data Fig. 1e, 1f), p62 (a protein regulating autophagic clearance of dysfunctional organelles/aggregates)-containing aggregates, ubiquitin (Ub)-positive inclusions (Extended Data Fig. 1g), increased p62 levels and reduced LC3II-accumulation after Baf treatment (Extended Data Fig. 1h, 1i) -common traits of deficient autophagy. Of note, 2-week-treatment with Rapamycin (or Spermidine), well-known autophagy-inducing regimes<sup>21,22</sup>, in old mice restored stem-cell basal autophagy (Fig. 1c; Extended Data Fig. 1j; Supplementary Video 3 and 4), reducing protein and organelle aggregates (Fig. 1d; Extended Data Fig. 1k).

### Autophagy reestablishment avoids senescence and restores regeneration in geriatric stem cells

Satellite cells at geriatric age (over 28 months in mice) enter a senescent state<sup>6,23</sup>. We investigated whether dysregulated basal autophagy may underlie loss of bona-fide quiescence. Using a mRFP-GFP-LC3 construct<sup>24</sup> (tandem-fluorescent-tagged LC3 reporter), transfected in young, old and geriatric satellite cells, in combination with Baf, we found a higher blockade of autophagic flux in geriatric than old cells, with respect to young cells. In the absence of Baf, red-color-labeled LC3 puncta (mature autolysosomes) were only abundant in young cells. Baf treatment induced yellow-color-labeled LC3 puncta (non-fused autophagosomes) accumulation in young cells, which was lower or blunted in old and geriatric cells (Fig. 2a). Geriatric satellite cells also showed increased colocalization of p62-ubiquitin aggregates in non-degraded autophagosomes (Fig. 2b). As p62 marks damaged organelles for degradation by selective autophagy, while Ub marks substrates for their degradation by both the ubiquitin-proteasome system (UPS) and

selective autophagy, the increased signal of both proteins and their colocalization demonstrates that the defect on autophagy in these cells is due, at least in part, to a block in autophagosomes/lysosomes clearance.

To investigate if restoring autophagy could rescue the cell-intrinsic irreversible cell-cycle and regenerative block of geriatric cells, we engrafted freshly-isolated GFP-labeled young and geriatric satellite cells (pre-treated with Rapamycin or control-vehicle) into pre-injured muscles of young-recipient mice. Autophagy reactivation significantly restored expansion of geriatric cells (expressing Pax7, Ki67, MyoD or Mgn) after 4-day engraftment (Fig. 2c; Extended Data Fig. 2a-c) and prevented senescence (geroconversion), as shown by p16<sup>INK4a</sup> and  $\gamma$ H2AX reduction (Extended Data Fig. 2d). Rapamycin (or Spermidine) treatment also decreased geriatric senescent cells ( $\beta$ -galactosidase-positive, SA- $\beta$ -gal<sup>+</sup>) (Extended Data Fig. 2e, 2f) and re-established proliferation (Extended Data Fig. 2e). More importantly, genetic-autophagy refueling, by overexpressing Atg7 (crucial for autophagosome formation) (Fig. 2c; Extended Data Fig. 2g, 2h) rescued the proliferative defect, while reducing senescence (Extended Data Fig. 2e). Furthermore, satellite cell transplantation and whole-muscle graft experiments demonstrated that the sole Atg7 introduction in geriatric satellite cells rescued their intrinsic regenerative capacity, allowing new muscle-fiber formation (Fig. 2c; Extended Data Fig. 2i, 2j).

### **Genetic autophagy inhibition in young quiescent satellite cells causes senescence entry**

To investigate if basal autophagy disruption causally breaks quiescence, we intercrossed Atg7-floxed mice with Pax7-Cre and Pax7-Cre<sup>ER</sup> mice, to impair autophagy constitutively (Atg7 <sup>$\Delta$ Pax7</sup>) or inducibly (Atg7 <sup>$\Delta$ Pax7ER</sup>) after tamoxifen administration). Intercrossing Atg7 <sup>$\Delta$ Pax7</sup> with GFP-LC3 mice (Atg7 <sup>$\Delta$ Pax7</sup>:GFP-LC3) confirmed loss of autophagosomes in quiescent Atg7-null satellite cells (Extended Data Fig. 3a, 3b). Importantly, the satellite cell pool was severely reduced in Atg7 <sup>$\Delta$ Pax7</sup> mice (Fig. 3a; Extended Data Fig. 3c). Tamoxifen administration to 3-month-old Atg7 <sup>$\Delta$ Pax7ER</sup> mice led to satellite cell loss after 30 days (Fig. 3b), indicating that basal autophagy is required for both establishment and maintenance of the adult quiescent stem cell population. Remaining Atg7 <sup>$\Delta$ Pax7ER</sup> satellite cells showed unexpected induction of p16<sup>INK4a</sup>, p21<sup>CIP1</sup> and p15<sup>INK4b</sup>, and DNA damage ( $\gamma$ H2AX<sup>+</sup> cells) –signs of premature aging (Fig. 3c, 3d; Extended Data Fig. 3d). Of note, Atg7 <sup>$\Delta$ Pax7</sup> satellite cells did not undertake mitotic or myogenic differentiation pathways (Extended Data Fig. 3e). Thus, loss of autophagy with aging may causally underlie the age-associated muscle stem cell numerical decline<sup>5,6,8-10,25</sup>.

In response to muscle injury, Pax7<sup>+</sup> cells from young Atg7 <sup>$\Delta$ Pax7</sup> mice showed reduced activation and expansion capacity (Fig. 3e; Extended Data Fig. 3f), and accelerated entry into deep senescence<sup>23,26</sup> (geroconversion<sup>27</sup>) in vivo and in vitro, as demonstrated by: SA- $\beta$ -gal<sup>+</sup>-staining (Fig. 3f),  $\gamma$ H2AX<sup>+</sup>, p16<sup>INK4a</sup><sup>+</sup> and phosphorylated-S6<sup>+</sup> cells, and regenerative failure, shown by reduced cell proliferation and size of regenerating fibers (Fig. 3g; Extended Data Fig. 3g-l). Confirming the cell-intrinsic regenerative failure, fewer GFP<sup>+</sup> fibers derived from Atg7-null satellite cells were found in transplantation experiments (Extended Data Fig. 3m, 3n), and this failure could not be rescued by Rapamycin (nor Spermidine) (Extended Data Fig. 3m-o).

## Mitophagy failure and ROS-induction drive senescence in autophagy-deficient satellite cells

How could loss of autophagy in young quiescent satellite cells induce premature aging? Genetic autophagy impairment in satellite cells caused rapid accumulation of p62/Ub-positive aggregates, and mitochondria and lysosomes (mitotracker, and lysotracker and Lamp1), as in aged cells (Fig. 4a, 4b; Extended Data Fig. 4a). There was also a lower proportion of healthy mitochondria in old (and Atg7<sup>ΔPax7ER</sup>) satellite cells, as revealed by reduced membrane potential (lower ratio TMRM/MitoTrackerGreen MFI) (Fig. 4a, 4b). Furthermore, mitophagy (cellular capacity to clear by autophagy damaged mitochondria) was defective in geriatric satellite cells, as indicated by mitochondria accumulation inside autophagosomes/lysosomes (through mitochondria/lysosomes (TOM20/Lamp1) colocalization) (Extended Data Fig. 4b). In vivo Rapamycin (or Spermidine) treatment of geriatric mice restored mitophagy in satellite cells (Extended Data Fig. 4b-f). Consistent with age-impaired mitophagy, young, but not geriatric, cells, were capable of eliminating CCCP-damaged mitochondria (Extended Data Fig. 4d, 4e).

How does altered mitophagy lead to satellite cell senescence with aging? We detected higher levels of reactive-oxygen species (ROS), Parkin (marking damaged mitochondria for degradation by mitophagy), and DNA-damage markers in Atg7-deficient satellite cells (Extended Data Fig. 5a, 5b; Fig. 3d, 3g; Extended Data Fig. 3h), associated to p16<sup>INK4a</sup> and pS6 induction (Fig. 3g; Extended Data Fig. 3g; Extended Data Fig. 4h). Higher ROS and ROS-mitochondria colocalization were also observed in geriatric satellite cells, correlating with impaired mitophagic flux (Fig. 5a; Extended Data Fig. 4g). Of note, Baf-induced autophagy block caused greater mitochondria accumulation in young cells, compared to geriatric and Atg7<sup>ΔPax7ER</sup> cells, paralleling ROS increase (Fig. 5b). To address their role, ROS were inhibited with Trolox (vitamin E analog) (Extended Data Fig. 5c). Trolox treatment of old GFP-LC3 mice increased GFP-LC3 puncta (after Baf-treatment) and reduced p62/Ub aggregates and mitochondria-ROS colocalization in GFP-LC3 satellite cells (Extended Data Fig. 4g; Extended Data Fig. 5d). Attenuation of autophagic block by ROS inhibition was further confirmed in Baf-treated aged cells through LC3-II accumulation (Extended Data Fig. 5e, 5f) and mRFP-GFP-LC3 tandem-reporter, which detected reduced autophagosomes (RFP<sup>+</sup>/GFP<sup>+</sup> puncta) and rescued autophagic flux (Extended Data Fig. 5g). Importantly, Trolox treatment prevented appearance of senescence markers (Fig. 5d, 5e), restored expansion (Fig. 5d), and rescued the cell-intrinsic proliferative/regenerative defect of geriatric satellite cells after transplantation (Fig. 5f; Extended Data Fig. 5h). Thus, increased ROS, resulting from impaired autophagy, drive satellite cell senescence in aged cells.

Loss of the polycomb repressive complex-1 (PRC1)-mediated H2A monoubiquitination of lysine119 (H2Aub) at INK4a locus drives p16<sup>INK4a</sup> induction in geriatric satellite cells<sup>6</sup> (Extended Data Fig. 5i). We found that Trolox treatment restored INK4a locus H2Aub modification in geriatric and Atg7-deficient satellite cells (Fig. 6a, 6b), resulting in p16<sup>INK4a</sup> repression, and this reduced senescence while promoting proliferation (Fig. 5c-e; Extended Data Fig. 5j; Fig. 6c). Notably, p16<sup>INK4a</sup> genetic-silencing with short-hairpin-RNA restored proliferation in Atg7<sup>ΔPax7</sup> satellite cells while reducing senescence-associated genes and SA-β-gal<sup>+</sup> cells, and augmenting their regenerative capacity (Extended Data Fig. 5k; Extended Data Fig. 6a, 6b). Thus, the ROS-induced p16<sup>INK4a</sup> axis links impaired autophagy and senescence in aging satellite cells.

## Human geriatric satellite cells exhibit autophagy defects that promote senescence

Skeletal muscles from geriatric individuals show sarcopenia and presence of senescent satellite cells (Extended Data Fig. 6c, 6d)<sup>6</sup>. As in mice, human satellite cells from geriatric individuals showed defective protein- and organelle-clearance, as evidenced by p62 and mitochondrial accumulation (Extended Data Fig. 6e, 6f) compared to young cells, which was tightly-associated with increased ROS levels (Extended Data Fig. 6f, 6g) and SA- $\beta$ -gal<sup>+</sup> cells (Extended Data Fig. 6h), consistent with reduced proliferative potential (Extended Data Fig. 6i). The causal role of impaired autophagy on the geroconversion of aging human satellite cells under proliferative pressure was sustained by the capacity of Rapamycin to revert the abnormal mitochondrial content, protein aggregates and ROS (Extended Data Fig. 6e, 6f), and senescence phenotype (Extended Data Fig. 6h-k). Thus, restoration of autophagy and organelle homeostasis in aged human satellite cells suffices to rescue senescence, as in murine satellite cells.

## DISCUSSION

In tissues with little turnover, reversible quiescence is the normal stem-cell state throughout life. However, quiescence is known to be progressively lost with aging due to systemic/niche- and intrinsic-factor alterations<sup>2,5</sup>. Recent studies showed that at geriatric age, the normal stem-cell quiescent state is substituted by an irreversible senescence state, which results in numerical and functional stem cell decline<sup>6</sup>. The mechanisms accounting for maintenance of quiescence, preservation of the stem cell pool and prevention of senescence during an individual's life remain largely unknown. Our results demonstrate that quiescent satellite cells are equipped with cytoprotective and cellular quality control mechanisms that actively repress the senescence program, thereby preserving cells' integrity and fitness. We provide evidence of loss of autophagy in satellite cells with aging, resulting in accumulation of damaged proteins and organelles, leading to senescence and stem cell exhaustion. Consistent with this, genetic inhibition of autophagy specifically in satellite cells of young mice caused rapid senescence entry, resulting in stem-cell numerical and functional exhaustion, and defective muscle regeneration. These findings came as a double-surprise considering that basal-autophagy decline in quiescent stem cells of physiologically aged mammalian organisms was not described before, and that autophagy was normally considered an effector pathway, rather than a cause, of senescence, particularly in oncogene-induced senescence<sup>28-31</sup>.

How can autophagy balance quiescence and senescence in muscle stem cells? Here we show that in adult resting muscle, quiescent stem cells attenuate proteotoxicity by maintaining high basal autophagy flux, constituting a homeostatic "clean up" process. This function is particularly critical in a non-dividing stem cell, where mitotic dilution of intracellular toxic debris does not take place<sup>17,32</sup>. Autophagy failure in aged resting stem cells leads to accumulation of damaged proteins and dysfunctional organelles, specially mitochondria, which generates enhanced ROS levels that cause DNA damage and senescence entry, consistent with previous studies<sup>33-39</sup>. Indeed, we uncover ROS as a key epigenetic regulator of the senescence-promoting gene p16<sup>INK4a</sup> in aging stem cells, by impeding PRC1-mediated lysine119 H2A-ubiquitination, the required epigenetic mark for INK4a locus silencing. Consistent with this, treatment of geriatric mice (and mice with satellite cell-specific Atg7 deficiency) with antioxidants not only restored PRC1-mediated INK4a locus repression and prevented satellite cell senescence, but also restored regenerative capacity. Importantly, signs of impaired autophagy and loss of proteostasis, correlating with senescence and defective myogenic functions, were also observed in human satellite cells from geriatric individuals.

At variance with our findings, a recent elegant study demonstrated that, upon in vitro stress, autophagy does not decline, but is even induced in hematopoietic stem cells (HSCs) with aging, consistent with maintenance of HSC number<sup>40</sup>. Thus, we propose that long-lived quiescent stem cells within low turn-over tissues primarily rely on autophagy to preserve fitness and avoid senescence, and that stem cells of skeletal muscle particularly lose this protection during aging (Extended Data Fig. 6f). Of interest, a recent study also reported the need of autophagy for activation of young satellite cells<sup>41</sup>.

Our studies thus demonstrate that autophagy is a decisive factor between the quiescence and senescence fate of muscle stem cells (Extended Data Fig. 6l). Although aging-induced senescence is often viewed as an inescapable and irremediable process, we provide evidence that in vivo restoration of constitutive autophagy (or neutralization of excessive ROS) averts intracellular damage accumulation, and prevents satellite cell

senescence and functional decline in old mice, as well as in aged human stem cells, reinforcing the notion that the intrinsic-aging clock in stem cells can be pharmacologically manipulated.

## REFERENCES

- 1 Cheung, T. H. & Rando, T. A. Molecular regulation of stem cell quiescence. *Nat Rev Mol Cell Biol* **14**, 329-340, (2013).
- 2 Garcia-Prat, L., Sousa-Victor, P. & Munoz-Canoves, P. Functional dysregulation of stem cells during aging: a focus on skeletal muscle stem cells. *The FEBS journal* **280**, 4051-4062, (2013).
- 3 Yin, H., Price, F. & Rudnicki, M. A. Satellite cells and the muscle stem cell niche. *Physiol Rev* **93**, 23-67, (2013).
- 4 Montarras, D., L'Honore, A. & Buckingham, M. Lying low but ready for action: the quiescent muscle satellite cell. *The FEBS journal* **280**, 4036-4050, (2013).
- 5 Chakkalakal, J. V., Jones, K. M., Basson, M. A. & Brack, A. S. The aged niche disrupts muscle stem cell quiescence. *Nature* **490**, 355-360, (2012).
- 6 Sousa-Victor, P. *et al.* Geriatric muscle stem cells switch reversible quiescence into senescence. *Nature* **506**, 316-321, (2014).
- 7 Sousa-Victor, P., Garcia-Prat, L., Serrano, A. L., Perdiguero, E. & Munoz-Canoves, P. Muscle stem cell aging: regulation and rejuvenation. *Trends Endocrinol Metab* **26**, 287-296, (2015).
- 8 Cosgrove, B. D. *et al.* Rejuvenation of the muscle stem cell population restores strength to injured aged muscles. *Nat Med* **20**, 255-264, (2014).
- 9 Bernet, J. D. *et al.* p38 MAPK signaling underlies a cell-autonomous loss of stem cell self-renewal in skeletal muscle of aged mice. *Nat Med* **20**, 265-271, (2014).
- 10 Price, F. D. *et al.* Inhibition of JAK-STAT signaling stimulates adult satellite cell function. *Nat Med* **20**, 1174-1181, (2014).
- 11 Cuervo, A. M. *et al.* Autophagy and aging: the importance of maintaining "clean" cells. *Autophagy* **1**, 131-140 (2005).
- 12 He, C. & Klionsky, D. J. Regulation mechanisms and signaling pathways of autophagy. *Annual review of genetics* **43**, 67-93, (2009).
- 13 Fukada, S. *et al.* Molecular signature of quiescent satellite cells in adult skeletal muscle. *Stem Cells* **25**, 2448-2459, (2007).
- 14 Liu, L. *et al.* Chromatin modifications as determinants of muscle stem cell quiescence and chronological aging. *Cell Rep* **4**, 189-204, (2013).
- 15 Pallafacchina, G. *et al.* An adult tissue-specific stem cell in its niche: a gene profiling analysis of in vivo quiescent and activated muscle satellite cells. *Stem cell research* **4**, 77-91, (2010).
- 16 Carnio, S. *et al.* Autophagy impairment in muscle induces neuromuscular junction degeneration and precocious aging. *Cell Rep* **8**, 1509-1521, (2014).
- 17 Rubinsztein, D. C., Marino, G. & Kroemer, G. Autophagy and aging. *Cell* **146**, 682-695, (2011).
- 18 Mizushima, N., Yamamoto, A., Matsui, M., Yoshimori, T. & Ohsumi, Y. In vivo analysis of autophagy in response to nutrient starvation using transgenic mice expressing a fluorescent autophagosome marker. *Mol Biol Cell* **15**, 1101-1111, (2004).
- 19 Klionsky, D. J. *et al.* Guidelines for the use and interpretation of assays for monitoring autophagy in higher eukaryotes. *Autophagy* **4**, 151-175 (2008).
- 20 Zhu, J., Dagda, R. K. & Chu, C. T. Monitoring mitophagy in neuronal cell cultures. *Methods Mol Biol* **793**, 325-339, (2011).
- 21 Mammucari, C. *et al.* FoxO3 controls autophagy in skeletal muscle in vivo. *Cell Metab* **6**, 458-471, (2007).
- 22 Morselli, E. *et al.* Spermidine and resveratrol induce autophagy by distinct pathways converging on the acetylproteome. *The Journal of cell biology* **192**, 615-629, (2011).
- 23 van Deursen, J. M. The role of senescent cells in ageing. *Nature* **509**, 439-446, (2014).



- 24 Kimura, S., Noda, T. & Yoshimori, T. Dissection of the autophagosome maturation process by a novel reporter protein, tandem fluorescent-tagged LC3. *Autophagy* **3**, 452-460 (2007).
- 25 Tierney, M. T. *et al.* STAT3 signaling controls satellite cell expansion and skeletal muscle repair. *Nat Med*, (2014).
- 26 Munoz-Espin, D. & Serrano, M. Cellular senescence: from physiology to pathology. *Nat Rev Mol Cell Biol* **15**, 482-496, (2014).
- 27 Blagosklonny, M. V. Selective anti-cancer agents as anti-aging drugs. *Cancer biology & therapy* **14** (2013).
- 28 Young, A. R. *et al.* Autophagy mediates the mitotic senescence transition. *Genes Dev* **23**, 798-803, (2009).
- 29 Narita, M. *et al.* Spatial coupling of mTOR and autophagy augments secretory phenotypes. *Science* **332**, 966-970, (2011).
- 30 Perez-Mancera, P. A., Young, A. R. & Narita, M. Inside and out: the activities of senescence in cancer. *Nature reviews. Cancer* **14**, 547-558, (2014).
- 31 Capparelli, C. *et al.* Autophagy and senescence in cancer-associated fibroblasts metabolically supports tumor growth and metastasis via glycolysis and ketone production. *Cell Cycle* **11**, 2285-2302, (2012).
- 32 Flach, J. *et al.* Replication stress is a potent driver of functional decline in ageing haematopoietic stem cells. *Nature* **512**, 198-202, (2014).
- 33 Kodama, R. *et al.* ROS-generating oxidases Nox1 and Nox4 contribute to oncogenic Ras-induced premature senescence. *Genes to cells : devoted to molecular & cellular mechanisms* **18**, 32-41, (2013).
- 34 Ramsey, M. R. & Sharpless, N. E. ROS as a tumour suppressor? *Nat Cell Biol* **8**, 1213-1215, (2006).
- 35 Ito, K. *et al.* Reactive oxygen species act through p38 MAPK to limit the lifespan of hematopoietic stem cells. *Nat Med* **12**, 446-451, (2006).
- 36 Lee, A. C. *et al.* Ras proteins induce senescence by altering the intracellular levels of reactive oxygen species. *The Journal of biological chemistry* **274**, 7936-7940 (1999).
- 37 Mandal, P. K., Blanpain, C. & Rossi, D. J. DNA damage response in adult stem cells: pathways and consequences. *Nat Rev Mol Cell Biol* **12**, 198-202, (2011).
- 38 Shao, L. *et al.* Reactive oxygen species and hematopoietic stem cell senescence. *International journal of hematology* **94**, 24-32, (2011).
- 39 Lerner, C. *et al.* Reduced mammalian target of rapamycin activity facilitates mitochondrial retrograde signaling and increases life span in normal human fibroblasts. *Aging cell* **12**, 966-977, (2013).
- 40 Warr, M. R. *et al.* FOXO3A directs a protective autophagy program in haematopoietic stem cells. *Nature* **494**, 323-327, (2013).
- 41 Tang, A. H. & Rando, T. A. Induction of autophagy supports the bioenergetic demands of quiescent muscle stem cell activation. *The EMBO journal*, (2014).

## ACKNOWLEDGEMENTS

We are indebted to Drs. G. Mariño for the generous gift of GFP-LC3 transgenic mice, C. Keller and M. Capecchi for Pax-Cre mouse lines, J. Ruberte for TEM-studies help, E. Masliah and K. Kosberg for Atg7 lentivirus; M. Raya, M. Jardí, and V. Lukesova, for their technical contributions, and very particularly J. Guerra for help in microarray experiments and P. Sousa-Victor for initial findings; J. Martín-Caballero (PRBB Animal Facility) O. Fornas (UPF/CRG FACS Facility) for technical help, and the KS Society for enlivening. The authors acknowledge funding from MINECO, Spain (SAF2012-38547, PLE2009-0124; SAF2009-08374), AFM, E-Rare/ERANET, Fundació Marató TV3, MDA, EU-FP7 (Myoage, Optistem and Endostem) and DuchennePP-NL. MM-V acknowledges funding from ISCIII, Spain (FIS-PS09/01267, FIS-PI13/02512, CP09/00184, PI14/01529) and CIBERNED; and MS from the European Union ERC (282310-MyoPHAGY) and Foundation Leducq. L.G.-P. was supported by a Predoctoral Fellowship from Programa de Formación de Personal Investigador (Spain).

**Author Contributions.** L.G.-P. designed and performed most experiments, analyzed data, interpreted results and wrote the manuscript. A.L.S and E.P. designed and performed experiments, and helped in interpreting results and editing the manuscript. M.M-V. and M.S. helped in designing/interpreting some experiments/results and editing the manuscript. L.O., V.R.-B. and S.G. performed some experiments and provided technical support. E. R. provided technical support in microscopy. J.R.-U. and E.B. performed ChIP experiments and helped interpreting results. P.M.-C. conceived the project, designed experiments, interpreted results and wrote the manuscript.

**Author Information.** Microarray data have been deposited into the NCBI Gene Expression Omnibus under accession number GSE70376. Reprints and permissions information is available at [www.nature.com/reprints](http://www.nature.com/reprints). The authors declare no competing financial interests. Readers are welcome to comment on the online version of the paper. Correspondence and requests for materials should be addressed to P.M.-C. ([pura.munoz@upf.edu](mailto:pura.munoz@upf.edu)).

## FIGURE LEGENDS

### Figure 1. Altered basal autophagy in aging muscle stem cells.

**a**, Number and cellular area occupied by punctate GFP-LC3 in quiescent satellite cells. Arrowheads: autophagic vesicles. **b**, Autophagy flux in cells from (a). Satellite cells were treated with vehicle or Bafilomycin (+Baf) for 4 h prior to analysis. Results expressed as relative variation of GFP-LC3 mean fluorescence intensity (MFI) in -/+Baf conditions. **c**, Autophagy flux in quiescent satellite cells from old GFP-LC3 mice 2-week-treated with Rapamycin or vehicle-control. Satellite cells -/+Baf treatment as (b). **d**, p62/ubiquitin (Ub) MFI of cells from (c). Data show mean  $\pm$  s.e.m. Comparisons by two-side Mann-Whitney U-test. P values indicated. Number of samples, a) n=51 (Young) and 106 (Old), 3 animals; b) n=20000 cells/animal, 3 animals; c) n=20000 cells/animal, 3 animals; d) n=36 (Control) and 39 (Rapamycin), 3 animals. Z projections. Scale bars 1.5  $\mu$ m except c, 5  $\mu$ m.

### Figure 2. Defective autophagy causes numerical and functional satellite cell decline in aging.

**a**, The mRFP-GFP-LC3 plasmid was transfected into young/old/geriatric satellite cells for detecting autophagosomes (yellow-signal) and their maturation into autolysosomes (red-signal) (see Methods), and subjected to -/+Baf treatment (as Fig. 1b). Percentage of double-positive-puncta (RFP<sup>+</sup>/GFP<sup>+</sup>) (autophagosomes) from total-puncta (RFP<sup>+</sup>/GFP<sup>+</sup>, RFP<sup>+</sup>, autophagosomes and autolysosomes). **b**, p62 and Ub-aggregates quantification in quiescent satellite cells from (a). Colocalization-staining area with respect to total-cellular area. Pearson's coefficient (r): correlation of intensity values of green-red-pixels in dual-channel images. Arrowheads: colocalization. **c**, Equal number of satellite cells from young/geriatric mice, LV-GFP-infected, treated 48h -/+Rapamycin, or LV-Atg7 infected, were transplanted into injured-mouse muscle, and analyzed 4 or 28 days later (for 28th-day-analysis, see Extended Data Fig. 2i; see also Extended Data Fig. 2j). Fourth-day-analysis: GFP and Pax7 immunostaining. GFP<sup>+</sup> cells/muscle field vs. transplanted-young cells. Data show mean  $\pm$  s.e.m. Comparisons by two-side Mann-Whitney U-test. P values indicated. Number of samples, a) n=21 (Young), 19 (Young+Baf), 30 (Old), 15 (Old +Baf), 21 (Geriatric) and 15 (Geriatric+Baf), 3 animals; b) n= 35 (Young), 66 (Old) and 104 (Geriatric), 3 animals; c) n=5 engraftments/group. Representative images are shown. Z projections. Scale bars, 5  $\mu$ m except c 50  $\mu$ m.

### Figure 3. Genetic impairment of autophagy disrupts satellite cell homeostasis.

**a**, Satellite cell quantification by Pax7-immunostaining in muscles of 3-month-old Atg7<sup>WT</sup> and Atg7 <sup>$\Delta$ Pax7</sup> mice. **b**, Mouse tamoxifen-treatment and satellite-cell-analysis scheme. Satellite cell quantification in Atg7<sup>WT</sup>/Atg7 <sup>$\Delta$ Pax7<sup>ER</sup></sup> mice after 30-day-tamoxifen-treatment as (a). **c** RT-qPCR of senescence markers in cells from (b), 7-days-after-tamoxifen treatment. **d**, Percentage  $\gamma$ H2AX<sup>+</sup> from total-Pax7<sup>+</sup> cells as (a). **e,f**, BrdU<sup>+</sup> and SA- $\beta$ -gal<sup>+</sup> cell quantification from (a). Arrowhead: positive-staining. **g**, Western-blotting in cells from (a). Quantification post-normalization. Data show mean  $\pm$  s.e.m. Comparisons by two-side Mann-Whitney U-test. P values indicated. Number of samples, a) n=5 animals/group; b-g) n=3 animals/group. Representative images are shown. Z projections. Scale bars, 250  $\mu$ m.

### Figure 4. Autophagy loss results in mitochondrial dysfunction and organelle, protein and ROS accumulation.

**a**, Lysosomes (Lamp1 and LysoTracker) and mitochondria (MitoTracker) quantification on satellite cells from Atg7<sup>WT</sup> and Atg7<sup>ΔPax7ER</sup> mice 1-month-after tamoxifen-treatment.. Membrane potential (MP): TMRM MFI and MitoTrackerGreen MFI ratio. **b**, Quantification as in (a) on young/old satellite cells. MP as (a). Data show mean ± s.e.m. Comparisons by two-side Mann-Whitney U-test. P values indicated. Number of samples, a,b) n=20000 cells/animal, 3 animals. Representative images are shown. Z projections. Scale bars, 5 μm.

**Figure 5. ROS inhibition prevents senescence in aged satellite cells.**

**a**, ROS quantification of young and old satellite cells by CellROX flow-cytometry. **b**, Mitochondria (MitoTracker) and ROS (CellROX) in satellite cells, 24h -/+Baf. Results represent increased MFI -/+Baf. Young satellite-cells' representative images. **c**, RT-qPCR of senescence markers -/+ Trolox. **d**, Quantification of BrdU<sup>+</sup> and SA-β-gal<sup>+</sup> cells from (c), pre-treated -/+Trolox, and cultured 96h. **e**, Western-blotting in cells -/+Trolox. **f**, Geriatric cells -/+Trolox 48h-pre-treated, were transplanted and analyzed as in Fig. 2c. Data show mean ± s.e.m. Comparisons by two-side Mann-Whitney U-test. P values. Number of samples, a,b) n=20000 cells/animal, 3 animals; c-e) n=3 animals/group; f) n=4 engraftments/group. Representative images are shown. Z projections. Scale bars, 5 μm except f 50 μm.

**Figure 6. Epigenetic control of p16<sup>INK4a</sup> expression by ROS in autophagy-impaired satellite cells.**

**a**, ChIP for H2AK119ub (H2Aub) in geriatric satellite cells, -/+48h Trolox treatment. **b**, H2Aub-ChIP for Atg7<sup>WT</sup>/Atg7<sup>ΔPax7</sup> satellite cells treated as in (a). **c**, Western-blotting/quantification for cells in (b). Data show mean ± s.e.m. Comparisons by two-side Mann-Whitney U-test. P values indicated. Number of samples, a-c) n=3 animals/group.

## ONLINE METHODS

### Mice

Male mice (C57BL/6 (wild-type, WT), LC3-GFP, the offspring of intercrossing Atg7<sup>flf</sup> with Pax7<sup>Cre</sup> and Pax7<sup>CreER</sup> lines) were used at different ages. GFP-LC3 mice were kindly provided by G. Mariño. Mice with Atg7 gene deletion in satellite cells, inducible or constitutive, were generated by breeding Atg7<sup>flf</sup> mice (previously described in<sup>42</sup>) with the Pax7<sup>Cre</sup> and Pax7<sup>CreER</sup> lines (kindly provided by C. Keller and M. Capecchi, respectively). All animal experiments were approved by the Catalan Government using sex-, age- and weight-matched littermate animals.

When needed, Cre activity was induced by intraperitoneal injection (one injection per day for 4 days) with 5mg/25G body weight of tamoxifen (Sigma; 10mg/ml in corn oil).

### Induction of muscle regeneration

Mice were anaesthetized with ketamine/xylazine (80/10 mg kg<sup>-1</sup>, intraperitoneally). Regeneration of skeletal muscle was induced by intramuscular injection of cardiotoxin (CTX, Latoxan; 10<sup>-5</sup> M) in the tibialis anterior (TA) muscle of the mice as described<sup>43</sup>. At the indicated times after injury, mice were sacrificed and muscles were dissected, frozen in isopentane cooled with liquid nitrogen, and stored at -80 °C until analysis. For GFP immunostaining samples, muscle were prefixed 2 h in PFA 2% at 4°C, and were embedded in Sucrose 15% O/V at 4°C and then frozen in isopentane cooled with liquid nitrogen.

### Satellite cell isolation by FACS

Muscles were mechanically disaggregated and dissociated in Ham's F10 media containing collagenase D 0.8% (Roche) and Trypsin-EDTA 0.125% at 37 °C for 25 min four times and then filtered. Cells were then incubated in lysis buffer (BD Pharm Lyse) for 10 min on ice, re-suspended in PBS with 2.5% goat serum and counted. PE-Cy7-conjugated anti-CD31 (Biolegend 102418), anti-CD11b (Biolegend 101215/16) and anti-Sca-1 (Biolegend 108113/14) antibodies were used to exclude the Lin (-) negative population and Alexa647-conjugated anti-CD34 (BD Pharmigen 560230) and PE-conjugated anti-α7-integrin (Ablab AB10STMW215) were used for double-positive staining of quiescent satellite cells. Cells were sorted using a FACS Aria II (BD). Isolated satellite cells were used either for RNA extraction or were cultured in Ham's F10 supplemented with 30% FBS and bFGF (0.025 µg ml<sup>-1</sup>) (growth medium) for proliferation assays or plated in glass slides (Thermo Scientific 177402) for immunostaining analysis.

### Flow cytometry analysis

FACS isolated satellite cells (see above) were stained with different dyes for flow cytometry analysis. Staining for mitochondria, lysosomes and ROS was performed by incubating cells at 37°C with 1 µM TMRM (T-668), 100 nM MitoTracker Green FM (M7514), 100 nM MitoTracker Red CMXRos (M7512), 500nM LysoTracker Green DND-26 (L7526) and 5µM CellROX Green Reagent (C10444), following manufacture's protocols (Invitrogen) and directly analyzed without fixing. Cell analysis was performed in FACS LSR Fortesa (Becton Dickinson). For mean fluorescence intensity (MFI) determination, we used the flow cytometry analysis software Flowlogic. MFI refers to the fluorescence

intensity of each event (in average) of the selected cell population, in the chosen fluorescence channel.

### **Whole transcriptome analysis of FACS sorted satellite cells**

FACS sorted satellite cells were collected in lysis buffer and RNA extraction was performed using RNeasy Micro kit (Qiagen). cDNA was used on a transcriptome analysis by Agilent SurePrint G3 Mouse GE 8x60K high density microarray slides, performed at the microarray Unit of CRG (Barcelona, Spain). Microarray analysis was performed with 3 animals each. Data was normalized using cyclic loess, and differentially expressed genes were identified using AFM 4.0<sup>44</sup> for all pairwise comparisons. Raw data was taken from the Feature Extraction output files and was corrected for background noise using the normexp method. To assure comparability across samples quantile normalization was used. Differential expression analysis was carried out on non control probes with an empirical Bayes approach on linear models (limma). Results were corrected for multiple testing according to the False Discovery Rate (FDR) method. Statistical analysis was performed with the Bioconductor project (<http://www.bioconductor.org/>) in the R statistical environment. Venn diagrams were generated using BioVenn<sup>45</sup>.

### **In vivo treatments**

Autophagy of aged C57BL/6 and GFP-LC3 mice was induced as follows: one group of mice was i.p. injected with 4mg/kg BW Rapamycin (LC Laboratories) or vehicle (DMSO) every other day for 2 weeks; a second group was i.p. injected with 30mg/kg BW Trolox (6-hydroxy-2,5,7,8-tetramethylchroman-2-carboxylic acid, Sigma) or vehicle (DMSO) daily for 2 weeks; and the third group of mice was treated with 3mM Spermidine (S2626 Sigma) in drinking water for 2 weeks.

### **Satellite cell engraftment**

Satellite cell transplants were performed as in Sousa-Victor et al., 2014<sup>6</sup>, following an adapted protocol<sup>46</sup>. Basically, quiescent FACS-isolated satellite cells were collected, re-suspended in 20% FBS HAM'S F10 medium and injected into muscles of recipient mice previously injured with CTX the day before. Recipient mice were SCID mice. For each mouse, 10,000 cells were injected. At 4 days (for proliferation, senescence analyses) or 1 month (muscle regeneration) after cell injections, engrafted muscles were collected and processed for muscle histology. Results are expressed as % of GFP+ cells counted per muscle section (being 100% the young cells control data).

### **In vitro treatments**

Experiments for in vitro rescue of defective autophagy in satellite cells were performed in 20% FBS-containing HAM'S F10 medium (Growth medium), and adding either Rapamycin (100ng/ml, LC Laboratories), Trolox (25µl/ml, Sigma), Spermidine (5µM, Sigma) or vehicle (DMSO) for 48 h. Mitochondrial, lysosomal, and ROS analyses or ChIP experiment were performed right after treatments, while proliferation assay (BrdU staining) and senescence analysis (SA-β-gal assay and determination of RNA, protein expression of senescence markers), were performed 96 h after treatments.

Satellite cell treatments for in vivo engraftment in injured muscles: Freshly FACS isolated satellite cells from resting muscle of young and geriatric mice were treated for 48 h with Rapamycin (100ng/ml, LC Laboratories), Trolox (25µl/ml, Sigma) or vehicle (DMSO) prior to engraftment into pre-injured muscles of recipient mice. For each mouse, 10,000 cells

were injected. At 4 days after cell injections, engrafted muscles were collected and processed for muscle histology.

Bafilomycin (10nM Sigma B1793) was used to block autophagy for 4 h at 37°C and to analyze autophagosome accumulation by FACS, immunostaining and Western blotting. CCCP (Carbonyl cyanide 3-chlorophenylhydrazone) (10μM Sigma C2759), which abolishes the link between the respiratory chain and the phosphorylation system in intact mitochondria, causes mitochondria uncoupling and was used to treat satellite cells in vitro for 1 h to induce the selective autophagy of CCCP-damaged mitochondria (mitophagy).

### **Plasmid transfection**

Freshly isolated cells were transfected with mRFP-GFP-LC3<sup>20</sup> plasmid using Lipofectamine 3000 (Invitrogen), and further treated for 48h with Trolox (25μl/ml, Sigma) or vehicle (DMSO) for analysis on glass slides (Thermo Scientific 177402). Cells were fixed with 4% paraformaldehyde (PFA) in PBS for 10 minutes and nuclei were stained with DAPI (Invitrogen). After washing, glass slides were mounted with Mowiol. Measuring autophagy flux through this method is based on the concept of lysosomal quenching of GFP. GFP is a stably folded protein and relatively resistant to lysosomal proteases. However, the low pH inside the lysosome quenches the fluorescent signal of GFP, which makes it difficult to trace the delivery of GFP-LC3 to lysosomes. In contrast, RFP exhibits more stable fluorescence in acidic compartments, and mRFP-LC3 can readily be detected in autolysosomes. By exploiting the difference in the nature of these two fluorescent proteins (i.e., lysosomal quenching of GFP fluorescence versus lysosomal stability of RFP fluorescence), autophagic flux can be morphologically traced with an mRFP-GFP-LC3 tandem construct<sup>20</sup>. With this tandem construct, autophagosomes and autolysosomes are labeled with yellow (i.e., mRFP and GFP) and red (i.e., mRFP only) signals, respectively.

### **Proliferation assay**

Satellite cells were labeled with BrdU (1.5 μg ml<sup>-1</sup>; Sigma) for 1 h. BrdU-labeled cells were detected by immunostaining using rat anti-BrdU antibody (Oxford Biotechnology; 1:500) and a specific secondary biotinylated goat anti-rat antibody (Jackson Immunoresearch; 1:250). Antibody binding was visualized using Vectastain Elite ABC reagent (Vector Laboratories) and DAB. BrdU-positive cells were quantified as percentage of the total number of cells analyzed.

### **Senescence-associated β-galactosidase activity**

Senescence-associated β-galactosidase (SA-β-gal) activity was detected in satellite cells using the Senescence β-Galactosidase Staining kit (Cell signaling), according to the manufacturer's instructions. SA-β-gal-positive cells were quantified as percentage of the total number of cells analyzed.

### **Lentivirus infection**

Freshly isolated satellite cells were ex vivo infected with distinct lentivirus for 12 h. Medium was replaced and cells were transplanted into injured muscle of recipient mice for in vivo analysis, or subjected to in vitro assays. LV-Atg7, used for Atg7 overexpression in satellite cells, was kindly provided by Eliezer Masliah's laboratory<sup>47</sup>. LV-sh p16<sup>INK4a</sup>, used to silence p16<sup>INK4a</sup>, and LV-sh Scramble (used as control), were previously described in Sousa-Victor et al, 2014<sup>5</sup>.

### Heterografting experiments

Extensor digitorum longus (EDL) muscles from geriatric WT mice were infected with Lentivirus (LV-Atg7 or LV-GFP, as well as LV-shp16<sup>INK4a</sup> or LV-sh Scramble) and grafted immediately onto the tibialis anterior (TA) muscle of young WT recipient mice, and regeneration (formation of new myofibers derived from EDL-associated satellite cells) in the transplanted EDL muscles was analyzed after 6 or 8 days. Fiber size of eMHC<sup>+</sup> myofiber was analyzed using Fiji program.

### RT-qPCR: RNA extraction, cDNA synthesis and PCR

Total RNA was isolated from either FACS-isolated satellite cells of mouse muscle tissue or human myoblasts obtained from human muscle biopsies, using Tripure reagent (Roche Diagnostic Corporation) or RNeasy Micro kit (Qiagen), and analysed by RT-qPCR. For qPCR experiments, DNase digestion of 10 mg of RNA was performed using 2 U DNase (Turbo DNA-free, Ambion). Complementary DNA (cDNA) was synthesized from total RNA using the First-Strand cDNA Synthesis kit (Amersham Biosciences). Real-time PCR reactions were performed on a LightCycler 480 System using Light Cyclor 480 SYBR Green I Master reaction mix (Roche Diagnostic Corporation) and specific primers. Thermocycling conditions were as follows: initial step of 10 min at 95 °C, then 50 cycles of 15 s denaturation at 94 °C, 10 s annealing at 60 °C and 15 s extension at 72 °C. Reactions were run in triplicate, and automatically detected threshold cycle (Ct) values were compared between samples. Transcript of the ribosomal protein L7 housekeeping gene was used as endogenous control, with each unknown sample normalized to L7 content. The following primers were used:

Gene	Forward primer	Reverse primer
p16 <sup>INK4a</sup>	CATCTGGAGCAGCATGGAGTC	GGGTACGACCGAAAGAGTTCCG
p21 <sup>CIP1</sup>	CCAGGCCAAGATGGTGTCTT	TGAGAAAGGATCAGCCATTGC
MyoD	GCCGCCTGAGCAAAGTGAATG	CAGCGGTCCAGGTGCGTAGAAG
Mgn	GGTGTGTAAGAGGAAGTCTGTG	TAGGCGCTCAATGTACTGGAT
Ki67	ACCGTGGAGTAGTTTATCTGGG	TGTTTCCAGTCCGCTTACTTCT
p15 <sup>INK4b</sup>	TCTTGCATCTCCACCAGCTG	CTCCAGGTTTCCCATTTAGC
Atg7	TCTGGGAAGCCATAAAGTCAGG	GCGAAGGTCAGGAGCAGAA

### Electron microscopy images

For electron microscopy images, tibialis anterior (TA) muscles from 3 and 24 month-old WT mice were fixed with 2% paraformaldehyde/2,5% glutaraldehyde in phosphate buffer (0.1M-pH7.4). Samples were processed by the CCit Microscopy Facility at the University of Barcelona. Images were acquired using a Jeol 1010 microscope, working at 80 kv and equipped with a CCD Megaview III camera. Identification of satellite cells in skeletal muscle by electron microscopy was based on cell size, content of heterochromatin and



position with respect to basal lamina.

### Western blotting

Preparation of mouse and human satellite cell lysates and Western blotting was performed as described previously by Perdiguero et al. 2007<sup>48</sup>. Antibodies used were: anti-p62/SQSTM1 antibody produced in rabbit (Sigma P0067), rabbit anti-LC3 (Novus Biologicals NB100-2331), phospho-S6 ribosomal protein (Ser240/244) XP™ Rabbit mAb (Cell Signaling 5364), rabbit anti-p16 (Santa Cruz Biotechnology sc-1207), rabbit anti-Parkin (Abcam ab15954), S6 ribosomal protein (54D2) mouse (Cell Signaling 2317), γH2AX Ser 139 (Cell Signaling 2577S), rabbit anti-53BP1 (Abcam ab21083) and Tubulin (Sigma T-6199).

### Chromatin Immunoprecipitation (ChIP)

Briefly, freshly isolated satellite cells were cultured with Trolox or vehicle (DMSO) for 48 h and cross-linked with 1% formaldehyde for 15 min at room temperature. For each ChIP, 300,000 cells were lysed in 130 μL of Lysis Buffer B (Low Cell ChIP Kit, Diagenode) and chromatin was sonicated for 10 min in a M220 Focused-ultrasonicator™, Covaris (Duty cycle 5%, Peak incident power 75 Watts and 200 cycles per burst). Sonicated chromatin was then diluted and subjected to immunoprecipitation with 3 μL of antibody against Ubiquityl-Histone H2A (Lys119) (D27C4) (Cell Signaling, 8240) or 3 μL of IgG. Bound fraction and input were analyzed by qPCR using specific primer sets for the INK4a locus.

Gene	Forward primer	Reverse primer
INK4a_RD	GGTCTCCCCTAGCAGGA	GCCTGTCATTAAACAGGGTGA
	TTC	
INK4a_exon1	CCGGAGCCACCCATTAA	CAAGACTTCTCAAAAATAAGACACT
	ACTA	GAAA
INK4a_exon2	CCCAACACCCACTTGAG	CAGAGGTCACAGGCATCGAA
	GAA	

### Histology and immunohistochemistry in muscle cryosections

Tibialis anterior (TA) and extensor digitorum longus (EDL) muscles were frozen in isopentane cooled with liquid nitrogen, and stored at -80 °C until analysis. 10 μm sections were collected from muscles and were either stained with hematoxylin/eosin (HE) or immunostained. Labelling of cryosections with mouse monoclonal primary antibodies was performed using the peroxidase or fluorescein M.O.M kit staining (Vector Laboratories) according to the manufacturer's instructions. Double immunostaining was performed by sequential addition of each primary and secondary antibody using appropriate positive and negative controls. Sections were air dried, fixed on PFA 2–4%, washed on PBS and incubated with primary antibodies according to manufacturer's instructions after blocking for 1 h at room temperature with a high protein-containing solution on PBS (Vector Laboratories). Subsequently, the slides were washed on PBS and incubated with appropriate secondary antibodies and labelling dyes. For immunofluorescence, secondary antibodies were coupled to Alexa-488, Alexa-568 or Alexa-647 fluorochromes, and nuclei were stained with DAPI (Invitrogen). After washing, tissue sections were mounted with

Mowiol.

### **Antibodies used for immunohistochemistry**

Immunohistochemistry on muscle cryosections or isolated satellite cells was performed with the following antibodies: GFP (Invitrogen A6455 and Aves labs GFP-1020), anti-eMHC (F1.652), anti-Pax7 (DSHB), p16 (Santa Cruz sc-1207),  $\gamma$ H2AX Ser 139 (2577S), rabbit polyclonal anti-MyoD (Santa Cruz Biotechnology sc-760), anti-myogenin (DSHB F5D), poly ubiquitinated proteins, multi ubiquitin chains, mouse mAb (Enzo life sciences PW8805), anti-p62/SQSTM1 antibody produced in rabbit (Sigma P0067), mouse monoclonal antibody to LC3 (NanoTools 5F10), LAMP-1 (Santa cruz Biotechnology sc-19992), phospho-S6 ribosomal protein (Ser240/244) XP<sup>TM</sup> Rabbit mAb (Cell Signaling 5364), anti-CD56 (BD Pharmingen 556325), anti-TOM20 (ab56783).

### **Human muscle samples**

Muscle biopsies from eight adults and ten geriatric ( $28 \pm 7$  and  $83 \pm 7$  years old, respectively) human subjects were obtained via the Tissue Banks for Research from Vall d'Hebron and Sant Joan de Deu Hospitals and especially via the EU/FP7 Myoage Consortium. Muscle biopsies were taken from the vastus lateralis muscle under local anaesthesia (2% lidocaine). A portion of the muscle tissue was directly frozen in melting isopentane and stored at  $-80^{\circ}\text{C}$  until analysis. Human primary myoblasts from 5 young/adult ( $25 \pm 4$  years old) and 5 geriatric ( $75 \pm 4$  years old) subjects were obtained from the EU/FP7 Myoage Consortium or purchased from Cook Myosite and cultured following the provided instructions.

### **Digital image acquisition and processing**

Digital images were acquired using: (1) an upright microscope DMR6000B (Leica) equipped with a DFC300FX camera for immunohistochemical color pictures and a Hamamatsu ORCA-ER camera for immunofluorescence pictures; (2) confocal images of muscle sections or isolated satellite cells were taken using either a Zeiss LSM-780 confocal system with a Plan-Apochromat 63x/1.4 oil objective or a Leica SPE confocal laser scanning microscope system with HCX PL Fluotar 10x/0.30, 20x/0.50 and 40x/0.75 objectives. The different fluorophores (3 to 4) were excited by using the 405, 488, 568 and 633 excitation lines. Acquisition was performed using Zeiss LSM software Zen Black or Leica Application or LAS AF software (Leica). Images were composed and edited in Photoshop CS5 (Adobe), where background was reduced using brightness and contrast adjustments applied to the whole image. To assess myofiber size, individual fibers were manually outlined and their cross-sectional area (CSA) was determined with the public domain image analysis software Fiji. Fluorescence intensity of selected proteins for each cell was quantified using Fiji software and the average of relative fluorescence was expressed as MFI.

The number and percentage of cellular area occupied by GFP-LC3 puncta were determined on digital images with Fiji and the cell image analysis software CellProfiler<sup>49</sup>. Colocalization of RFP-LC3 and GFP-LC3 puncta was determined on the maximum projection of three Z-sections using a Fiji automated macro pipeline calculating single and double-positive autophagosomes. Colocalization of p62/Ub was determined on digital images Fiji, according to<sup>50</sup>, with respect to the total cellular area. The Pearson's coefficient (r) was used to analyze the correlation of the intensity values of green and red pixels in

dual-channel images. This coefficient measures the strength of the linear relationship between the intensities in two images calculated by linear regression and ranges from 1 to -1, with 1 standing for complete positive correlation and -1 for a negative correlation, with zero standing for no correlation<sup>49</sup>. Video reconstructions of autophagosomes were generated in Imaris software using full confocal z-stacks (around 20) of each cell. Z-stacks were previously imported to Fiji software for background adjustments and then deconvolved using the blind-deconvolution wizard of Huygens software.

### **Statistical analysis**

For mouse experiments, no specific blinding method was used but mice in each sample group were selected randomly. The sample size (n) of each experimental group is described in each corresponding figure legend, and all experiments were repeated at least with three biological replicates. GraphPad Prism software was used for all statistical analyses. Quantitative data displayed as histograms are expressed as means  $\pm$  standard error of the mean (represented as error bars). Results from each group were averaged and used to calculate descriptive statistics. Mann–Whitney U-test (independent samples, two-sided) was used for pairwise comparisons among groups at each time point. Statistical significance was set at a P value  $<0.05$ .

- 42 Masiero, E. *et al.* Autophagy is required to maintain muscle mass. *Cell Metab* **10**, 507-515, (2009).
- 43 Suelves, M. *et al.* uPA deficiency exacerbates muscular dystrophy in MDX mice. *The Journal of cell biology* **178**, 1039-1051, (2007).
- 44 Breitkreutz, B. J., Jorgensen, P., Breitkreutz, A. & Tyers, M. AFM 4.0: a toolbox for DNA microarray analysis. *Genome biology* **2**, SOFTWARE0001 (2001).
- 45 Hulsen, T., de Vlieg, J. & Alkema, W. BioVenn - a web application for the comparison and visualization of biological lists using area-proportional Venn diagrams. *BMC Genomics* **9**, 488, (2008).
- 46 Sacco, A. *et al.* Short telomeres and stem cell exhaustion model Duchenne muscular dystrophy in mdx/mTR mice. *Cell* **143**, 1059-1071, (2010).
- 47 Crews, L. *et al.* Selective molecular alterations in the autophagy pathway in patients with Lewy body disease and in models of alpha-synucleinopathy. *PLoS One* **5**, e9313, (2010).
- 48 Perdiguero, E. *et al.* Genetic analysis of p38 MAP kinases in myogenesis: fundamental role of p38alpha in abrogating myoblast proliferation. *The EMBO journal* **7**, 1245-1256. (2007).
- 49 Kamentsky, L. *et al.* Improved structure, function and compatibility for CellProfiler: modular high-throughput image analysis software. *Bioinformatics* **27**, 1179-1180, (2011).
- 50 Bolte, S. & Cordelieres, F. P. A guided tour into subcellular colocalization analysis in light microscopy. *Journal of microscopy* **224**, 213-232, (2006).

## EXTENDED DATA

### **Extended Data 1. The reduced autophagy flux in quiescent satellite cells can be pharmacologically refueled in vivo.**

**a**, Venn diagrams of overlapping genes between a proteostasis gene set (See Supplementary Table 1) and genes significantly upregulated in quiescent satellite cells from the indicated publications or from our gene expression microarray data comparing freshly FACS isolated satellite cells from resting muscle, or muscle injured with cardiotoxin (CTX) for 72 h, from young WT mice. **b**, K-means clustering analysis (performed with Gene-E, Broad Institute) of the gene expression of the autophagy-related genes during aging. Clusters are shown with heat maps of the normalized raw data. Each column represents a different sample and each row a different gene probe. Red, increased expression; white, neutral expression; blue, decreased expression. **c**, Representative example of the FACS strategy and gating scheme to isolate satellite cells from mice in resting conditions. **d**, Pax7 and GFP immunostaining of freshly isolated satellite cells from resting muscles of young and old GFP-LC3 mice. Scale bar, 5  $\mu$ m. **e**, Electron microscopy images of young and old satellite cells on sections of resting tibialis anterior (TA) muscle of WT mice. Arrowheads indicate autophagic vesicles. Scale bar, 1 and 0.5  $\mu$ m (right and left, respectively). **f**, Pax7 and GFP immunostaining on tissue sections from resting TA muscles of young and old GFP-LC3 mice. Arrowheads indicate autophagic vesicles. Scale bar, 5  $\mu$ m. **g**, p62/ubiquitin (Ub) MFI. Arrowheads: p62/Ub-aggregates colocalization. **h**, LC3 Western blot of freshly isolated satellite cells from young and old WT mice, treated with Bafilomycin (+Baf) or vehicle for 4 h prior to collection. Graph shows LC3II quantification, after normalization with Tubulin levels. **i**, p62 Western blotting of freshly isolated satellite cells from young and old WT mice. Graph shows p62 quantification, after normalization with Tubulin levels. **j**, Quiescent satellite cells were freshly isolated from old WT mice subjected to 2-week Rapamycin, Spermidine or vehicle (control) treatment. Cells were treated or not with Bafilomycin 4 h prior analysis by immunostaining of LC3 marker. Z projections of representative fluorescence microscopy images are shown. Scale bar, 5  $\mu$ m. **k**, Representative fluorescent microscopy images from Fig. 1d. Scale bar, 5  $\mu$ m. Data show mean  $\pm$  s.e.m. Comparisons by two-side Mann-Whitney U-test. P values are indicated. Number of samples, a,b) n=3 animals/group; g) n=35 (Young) and 66 (Old), 3 animals; h,i) n=3 animals/group.

### **Extended Data 2. Reinduction of autophagy rescues proliferation and reduces senescence in geriatric satellite, thus restoring regenerative capacity.**

**a**, Transplanted muscles from Fig. 2c were immunostained for GFP and for Ki67/Pax7/MyoD/Mgn (to decipher the distinct possible myogenic states of satellite cells in the regenerating muscle). Scale bar, 50  $\mu$ m. **b**, Autophagy flux analyzed by flow cytometry in freshly isolated satellite cells from resting muscle of GFP-LC3 mice, treated for 48 h with Rapamycin or vehicle (control). Satellite cells were treated with Bafilomycin (+Baf) or vehicle for 4 h prior to analysis. Results are expressed as a relative variation of GFP-LC3 MFI in -Baf compared to +Baf conditions. **c**, Western blot analysis of phospho-S6 (pS6) protein levels in young and geriatric satellite cells from WT mice, treated for 48 h with Rapamycin or vehicle (control). Graph shows pS6 quantification, normalized to Tubulin. **d**, As in Fig. 2c, percentage  $\square$ H2AX<sup>+</sup>/GFP<sup>+</sup> or p16<sup>INK4a</sup>/GFP<sup>+</sup> cells from total-GFP<sup>+</sup> cells are quantified. Scale bar, 10  $\mu$ m. **e**, Quantification BrdU<sup>+</sup> and SA- $\beta$ -gal<sup>+</sup> satellite cells, pre-treated as in Fig. 2c and analysed after 96h. **f**, Quantification of senescent (SA- $\beta$ -gal<sup>+</sup>)

satellite cells, isolated from young and geriatric WT mice, pre-treated for 48 h with Spermidine or vehicle (control) and cultured for 96 h. **g**, Quantitative real-time PCR (RT-qPCR) analysis of Atg7 expression on satellite cells infected with LV-Atg7 or LV-control (LV-Co), and cultured for 96 h. **h**, GFP-LC3 satellite cells were infected with LV-Atg7 or LV-Co and treated with Bafilomycin (+Baf) or vehicle for 4 h prior to analysis. Autophagy flux was analyzed by flow cytometry and represented as in (b). Representative images are shown. Scale bar, 10  $\mu$ m. **i**, Muscle regeneration experiment by satellite cell transplantation: Equal number of satellite cells from young and geriatric mice infected with a lentivirus overexpressing Atg7 gene (LV-Atg7) or a lentivirus control (LV-Co), which also expressed GFP, were transplanted into injured muscle of young immunodeficient mice, and collected 28 days later. GFP expression in muscles was analyzed by immunostaining. Quantification of GFP<sup>+</sup> cells (fibers) per muscle field vs. transplanted control-treated satellite cells and representative images are shown. Scale bar, 75  $\mu$ m. **j**, EDL geriatric muscles, infected with LV-Atg7 or LV-Co, and grafted on recipient mouse-muscle, and regeneration analyzed 8-days-later. Frequency distribution of regenerating fibers by size. Scale bar, 25  $\mu$ m. Data as mean  $\pm$  s.e.m. Comparisons by two-side Mann-Whitney U-test. P values are indicated. Number of samples, b) n=20.000 cells/animal, 3 animals; c) n=3 animals/group; d) n=5 engraftments/group; e-g) n=3 animals/group; h) n=20.000 cells/animal, 3 animals; i) n=3 engraftments/group; j) n=4 engraftments/group.

### **Extended Data 3. Genetic impairment of autophagy in young quiescent satellite cells leads to premature senescence and impaired muscle regeneration.**

**a**, RT-qPCR analysis of Atg7 expression and Western blot analysis of LC3, p62 and Tubulin of satellite cells isolated from Atg7<sup>WT</sup> and Atg7 <sup>$\Delta$ Pax7</sup> mice. Graph shows the quantification of p62 normalized to Tubulin. **b**, Quiescent satellite cells were freshly isolated from Atg7<sup>WT</sup> and Atg7 <sup>$\Delta$ Pax7</sup> mice which had been subjected to 2-week Rapamycin or vehicle (control) treatment in vivo. Cells were treated or not with Bafilomycin 4 h prior analysis by fluorescence microscopy. Z projections of representative fluorescence microscopy images are shown. Scale bar, 5  $\mu$ m. **c**, Quantification of satellite cells in resting muscle of 3 month-old Atg7<sup>WT</sup> and Atg7 <sup>$\Delta$ Pax7</sup> mice by flow cytometry analysis ( $\alpha$ 7integrin<sup>+</sup> CD34<sup>+</sup> cells per gram of muscle tissue). **d**, Representative fluorescent microscopy images from Fig. 3d. Scale bar, 10  $\mu$ m. **e**, RT-qPCR analysis of MyoD, Myogenin (Mgn), and Ki67 expression in freshly isolated quiescent satellite cells from resting muscle of Atg7<sup>WT</sup> and Atg7 <sup>$\Delta$ Pax7<sup>ER</sup></sup> mice, 7 days after tamoxifen treatment. **f**, Percentage of activated-satellite cells (Pax7<sup>+</sup>/MyoD<sup>+</sup>) from total-Pax7<sup>+</sup> cells (FACS-isolated 14-h post-injury from (a)). Scale bar, 50  $\mu$ m. **g**, pS6/Lamp1-immunostaining of cells from (a). Scale bar, 10  $\mu$ m. **h**,  $\gamma$ H2AX protein levels per nucleus on Pax7<sup>+</sup> satellite cells in TA muscles of Atg7<sup>WT</sup> and Atg7 <sup>$\Delta$ Pax7<sup>ER</sup></sup> mice, 15 days post-injury. Representative images are shown. Scale bar, 25  $\mu$ m. **i**, Pax7<sup>+</sup> satellite cells were quantified following immunostaining on regenerating muscles of Atg7<sup>WT</sup> and Atg7 <sup>$\Delta$ Pax7<sup>ER</sup></sup> mice 7 and 15 days post cardiotoxin (CTX) injury. **j**, Representative images of hematoxylin/eosin staining of muscles at 7 days post-injury on muscles of Atg7<sup>WT</sup> and Atg7 <sup>$\Delta$ Pax7<sup>ER</sup></sup> mice. Fiber size of central-nucleated myofibers at 7 and 28 days post-injury is quantified. Scale bar, 50  $\mu$ m. **k**, TA muscles of Atg7<sup>WT</sup> and Atg7 <sup>$\Delta$ Pax7</sup> mice were injured by CTX injection and, 21 days after, these muscles were reinjured and analyzed 21 days later (21+21 days post-injury). The size of central-nucleated myofibers was quantified. Representative images are shown. Scale bar, 50  $\mu$ m. **l**, Pax7<sup>+</sup>/Ki67<sup>+</sup> satellite cells were quantified following immunostaining on regenerating muscles of Atg7<sup>WT</sup> and Atg7 <sup>$\Delta$ Pax7<sup>ER</sup></sup> mice 7 days post

cardiotoxin (CTX) injury. **m**, Equal number of quiescent satellite cells from Atg7<sup>WT</sup>:GFP-LC3 and Atg7<sup>ΔPax7</sup>:GFP-LC3 mice (2-weeks +/-Rapamycin-pre-treated), transplanted as in Fig. 2c, and immunostained with indicated-antibodies 4-days-later. Quantification GFP<sup>+</sup>cells/muscle field vs. transplanted young WT satellite cells. Representative images are shown. Scale bar, 75 μm. **n**, Percentage of GFP+/Ki67+ from total GFP+ cells in muscles from (m). **o**, Quantification of proliferating (BrdU<sup>+</sup>) and senescent (SA-β-gal<sup>+</sup>) satellite cells, isolated from Atg7<sup>WT</sup> and Atg7<sup>ΔPax7</sup>, pre-treated for 48 h with Spermidine or Rapamycin (or control vehicle) and cultured for 96 h. Data show mean ± s.e.m. Comparisons by two-side Mann-Whitney U-test. P values are indicated. Number of samples, a) n=3 animals/group; c) n=7 animals/group; e-l) n=3 animals/group; m,n) n=4 engraftments/group; o) n=3 animals/group.

#### **Extended Data 4. Autophagy loss in satellite cells causes dysfunctional mitophagy and mitochondria accumulation, leading to increased ROS and senescence.**

**a**, p62 and ubiquitin (Ub) immunostaining on freshly isolated satellite cells from resting muscle of 3 month-old Atg7<sup>WT</sup> and Atg7<sup>ΔPax7<sup>ER</sup></sup> mice, 1-month-after tamoxifen-treatment. Arrowheads indicate colocalization of p62 and Ub aggregates. Representative images are shown. Scale bar, 5 μm. **b**, TOM20 and Lamp1 immunostaining on quiescent satellite cells isolated from young and geriatric WT mice. Mice were subjected to 2-week Rapamycin, Spermidine or Trolox (or vehicle) treatment prior to analysis. Colocalization was calculated as the area occupied by the immunofluorescence co-localizing staining on pictures with respect to the total cellular area. The Pearson's coefficient (r) was used to analyze the correlation of the intensity values of green and red pixels in dual-channel images. Z projections of representative fluorescence microscopy images are shown. Scale bar, 5 μm. **c**, Mitochondria quantification by MitoTracker in quiescent satellite cells of old mice, treated with Rapamycin or vehicle for two weeks. **d**, Mitochondria (MitoTracker) in young/geriatric cells. Satellite cells, pre-treated with CCCP for 1h (see Methods), and +/-Rapamycin for 24h. Percentage of MitoTracker MFI reduction +/-Rapamycin. **e**, Mitochondrial membrane potential (MP) analysis: Satellite cells were freshly isolated from young WT mice and treated for 1h with CCCP or DMSO (Control). Membrane potential (TMRM MFI/MitoTrackerGreen MFI ratio) of cells was calculated by flow cytometry analysis at 1h and 24h after CCCP treatment (being 100% the MP value of control satellite cells). **f**, Mitochondria content was quantified by MitoTracker staining of satellite cells from young and geriatric WT mice and treated with Rapamycin or vehicle (control) for 48 h. Z projections of representative fluorescence microscopy images are shown. Scale bar, 5 μm. **g**, Mitochondria and ROS detection by MitoTracker and CellROX staining, respectively. Colocalization was calculated as in (b). Z projections of representative fluorescence microscopy images are shown. Scale bar, 5 μm. **h**, Representative images of freshly isolated satellite cells from resting muscle of 3 month-old Atg7<sup>WT</sup> and Atg7<sup>ΔPax7</sup> mice stained with CellROX fluorescent dye and p16<sup>INK4a</sup> antibody. Scale bar, 5 μm. Data show mean ± s.e.m. Comparisons by two-side Mann-Whitney U-test. P values are indicated. Number of samples, a) n=36 (Atg7<sup>WT</sup>) and n=38 (Atg7<sup>ΔPax7<sup>ER</sup></sup>), 3 animals; b) n=23 (Young), 24 (Control), 42 (Rapamycin); 28 (Spermidine) and 21 (Trolox), 3 animals; c) n=20000 cells/animal, 3 animals; d) n=10000 cells/animal, 4 animals; e,f) n=10000 cells/animal, 3 animals; g) n=18 (Young), 21 (Control), 15 (Rapamycin) and 13 (Trolox), 3 animals.

#### **Extended Data 5. ROS in autophagy-impaired aged and Atg7-null satellite cells**

**significantly restores cell proteostasis.**

**a**, ROS-level quantification in quiescent satellite cells from 3 month-old Atg7<sup>WT</sup> and Atg7<sup>ΔPax7</sup> mice by CellROX flow-cytometry. Representative images are shown. Scale bar, 5 μm. **b**, Western blot analysis of 53BP1 and Parkin in satellite cells isolated from 3 month-old Atg7<sup>WT</sup> and Atg7<sup>ΔPax7</sup> mice. Tubulin control is common for Fig. 3g. Graph shows quantification of 53BP1 and Parkin protein normalized to Tubulin. **c**, ROS levels quantification on satellite cells isolated from young and geriatric WT mice by flow cytometry using CellROX fluorescent dye. Satellite cells were treated with Trolox or vehicle (control) for 48 h before analysis. Results are represented as variation of MFI between young and geriatric satellite cells. **d**, Quantification of p62 and ubiquitin (Ub) protein levels on immunostained freshly isolated satellite cells from resting muscle of old WT mice, in vivo treated for 2 weeks with Trolox or vehicle (control). Representative images are shown. Scale bar, 5 μm. **e**, Western blot analysis of LC3 and Tubulin in satellite cells isolated from geriatric WT mice and treated for 48 h with Trolox or vehicle (control), in the absence or presence of Bafilomycin (+Baf) for 4 h prior to analysis. Graph shows quantification of LC3II protein normalized to Tubulin. **f**, Autophagy flux and mitochondria in satellite cells from GFP-LC3 mice (2-weeks +/-Trolox-treated). Satellite cells 4h +/-Baf. Representative images are shown. Scale bar, 5 μm. **g**, mRFP-GFP-LC3 plasmid was transfected into young/geriatric satellite cells, 48h-treated +/-Trolox, and 4h +/-Baf, prior fixation. Autophagosomes' percentage quantified as in Fig. 2a. **h**, Muscle regeneration experiment by geriatric satellite cell transplantation. Equal number of freshly-isolated geriatric satellite cells, infected with GFP lentivirus, and treated for 48 h with Trolox or vehicle, were transplanted into injured muscle of young immunodeficient mice. Four days later, muscles were collected and immunostained for GFP, MyoD and Mgn (to decipher the distinct possible myogenic states of satellite cells in the regenerating muscle). Representative images are shown. Scale bar, 50 μm. **i**, ChIP analysis for H2AK119ub (H2Aub) in satellite cells isolated from young and geriatric WT mice. **j**, Quantification of proliferating (BrdU<sup>+</sup>) and senescent (SA-β-gal<sup>+</sup>) satellite cells isolated from Atg7<sup>WT</sup> and Atg7<sup>ΔPax7</sup> mice treated 48 h with Trolox or vehicle (control) and cultured for 96 h. **k**, Quantification of proliferating (BrdU<sup>+</sup>) and senescent (SA-β-gal<sup>+</sup>) satellite cells isolated from Atg7<sup>WT</sup> and Atg7<sup>ΔPax7</sup> mice and infected with LV-sh p16<sup>INK4a</sup> or LV-sh Scramble, and cultured for 96 h. Data show mean ± s.e.m. Comparisons by two-side Mann-Whitney U-test. P values are indicated. Number of samples, a) n=20000 cells/animal, 3 animals; b) n=3 animals/group; c) n=20000 cells/animal, 3 animals; d) n=36 (Control) and n=35 (Trolox), 3 animals; e) n=3 animals/group; f) n=20000 cells/animal, 3 animals; g) n=21 (Young), 20 (Young Trolox), 19 (Young+Baf), 18 (Young Trolox +Baf), 21 (Geriatric), 19 (Geriatric Trolox), 15 (Geriatric+Baf) and 37 (Geriatric Trolox +Baf), 3 animals; i-k) n=3 animals/group.

**Extended Data 6. Effects of p16<sup>INK4a</sup> silencing in autophagy-impaired young murine satellite cells, and evidence of impaired autophagic flux in human geriatric satellite cells.**

**a**, Western-blotting/quantification of Atg7<sup>ΔPax7</sup> satellite cells, infected with lentiviral LV-sh-p16<sup>INK4a</sup> or LV-sh-Scramble, analyzed 96h later. **b**, Atg7<sup>WT</sup> and Atg7<sup>ΔPax7</sup> EDL, infected with LV-sh-p16<sup>INK4a</sup> or LV-sh-Scramble, and grafted as Fig. 2f. Representative eMHC-immunostaining. Scale bar, 25 μm. **c**, Representative images of hematoxylin/eosin (H/E) staining of human muscle biopsies from young (25 years) and geriatric (95 years) donors in resting conditions. Arrowheads indicate atrophic myofibers. Scale bar, 50 μm. **d**, CD56



and p16<sup>INK4a</sup> immunostaining on human muscle sections of samples described in (a). Scale bar, 10  $\mu$ m. **e**, Western-blotting analysis of p62 protein in human satellite cells from young (about 25-years) and geriatric (over 75-years) donors, 48h-treated -/+Rapamycin. **f**, ROS and mitochondria content analysis in human cells from treated for 48h -/+Rapamycin. Graphs: MFI variation. Scale bar, 5  $\mu$ m. **g**, Representative images from CellROX staining from (f). Scale bar, 5  $\mu$ m. **h**, Quantification SA- $\beta$ -gal<sup>+</sup> human cells 48h-treated -/+Rapamycin. Quantification was done 96 h after treatment. Scale bar, 200  $\mu$ m. **i**, Quantification of proliferating (BrdU<sup>+</sup>) young and geriatric human satellite cells in culture. Representative pictures are shown. Scale bar, 25  $\mu$ m. **j**, Western blot analysis of pS6, total S6 and Tubulin in young and geriatric human satellite cells treated 48 h with Rapamycin or vehicle (control). Graphs show p62 quantification normalized to Tubulin. **k**, Immunostaining of pS6 in young and geriatric human satellite cells treated as in (j). Scale bar, 75  $\mu$ m. **l**, Scheme showing the proposed model of how age-impaired autophagy leads to muscle stem cell senescence and regenerative decline. Data show mean  $\pm$  s.e.m. Comparisons by two-side Mann-Whitney U-test. P values are indicated. Number of samples; a) n=3 animals/group; b) n=4 engraftments/group; e-j) n=3 human donors/group.

## **SUPPLEMENTARY INFORMATION GUIDE**

**Supplementary Table 1.** Gene list of proteostasis pathways and genes; Dataset of upregulated genes in quiescent muscle stem cells; Gene list of quiescence genes belonging to each proteostasis pathway, including autophagy

**Supplementary Video 1. 3D reconstruction of a young satellite cell from GFP-LC3 mice.**

Quiescent young satellite cells were isolated by FACS from 3-months old GFP-LC3 mice and fixed on glass slides for fluorescence microscopy analysis. 30 z stacks approximately were taken for video reconstruction as explained in the Methods section.

**Supplementary Video 2. 3D reconstruction of an old satellite cell from GFP-LC3 mice.**

Quiescent old satellite cells were isolated by FACS from 24-months old GFP-LC3 mice and fixed on glass slides for fluorescence microscopy analysis. 30 z stacks approximately were taken for video reconstruction as explained in the Methods section.

**Supplementary Video 3. 3D reconstruction of an old satellite cell from GFP-LC3 mice treated with vehicle (control) and Bafilomycin 4 hours prior fixation.**

Quiescent old satellite cells were treated for 4 hours with Bafilomycin and were isolated by FACS from 24-months old GFP-LC3 mice treated with vehicle (control) (i.e., the control of the Rapamycin treatment in Video 4) for two weeks in vivo. After sorting, satellite cells were fixed on glass slides for fluorescence microscopy analysis. 30 z stacks approximately were taken for video reconstruction as explained in the Methods section.

**Supplementary Video 4. 3D reconstruction of an old satellite cell from GFP-LC3 mice treated with Rapamycin and Bafilomycin 4 hours prior fixation.**

Quiescent old satellite cells were treated for 4 hours with Bafilomycin and were isolated by FACS from 24-months old GFP-LC3 mice treated with Rapamycin for two weeks in vivo. After sorting, satellite cells were fixed on glass slides for fluorescence microscopy analysis. 30 z stacks approximately were taken for video reconstruction as explained in the Methods section.



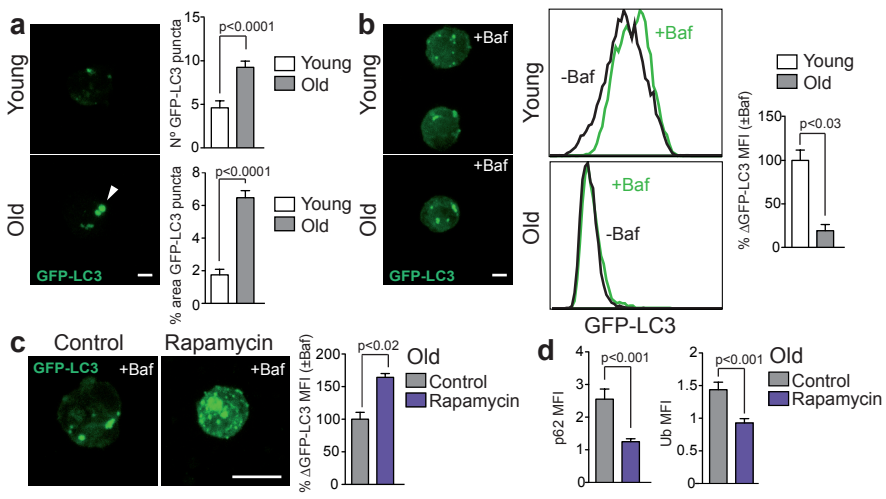


Figure 1

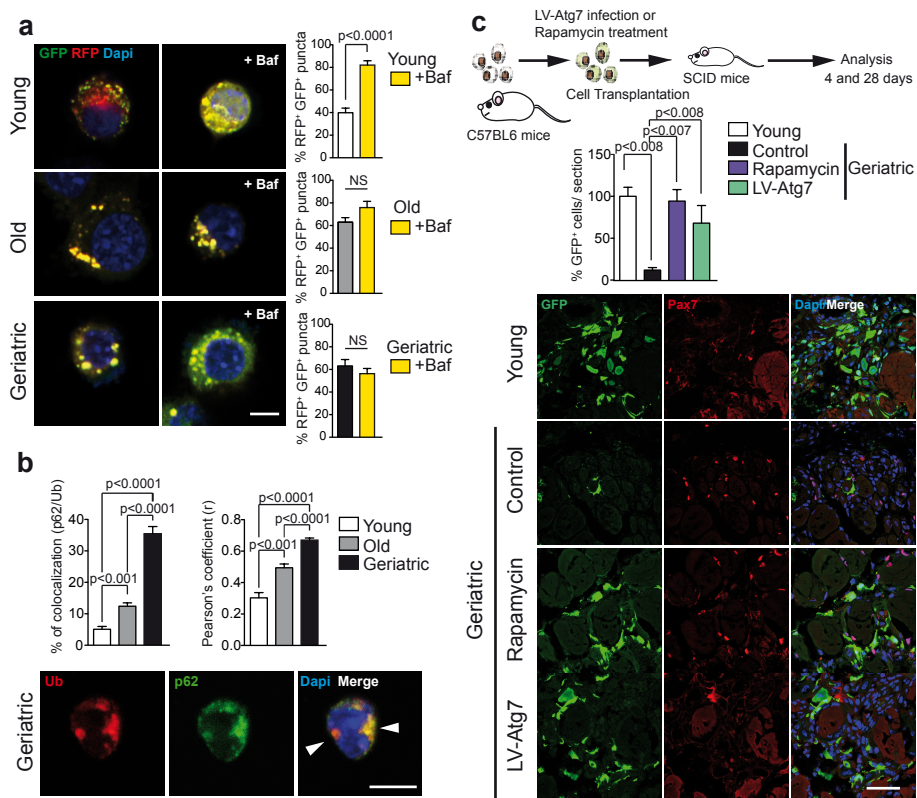


Figure 2

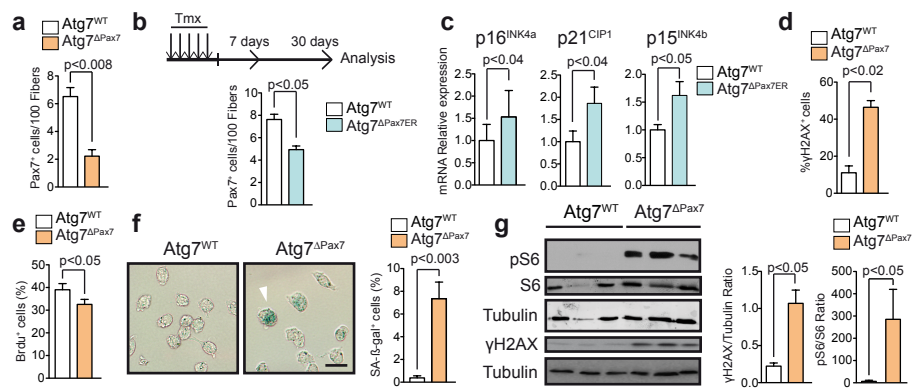


Figure 3

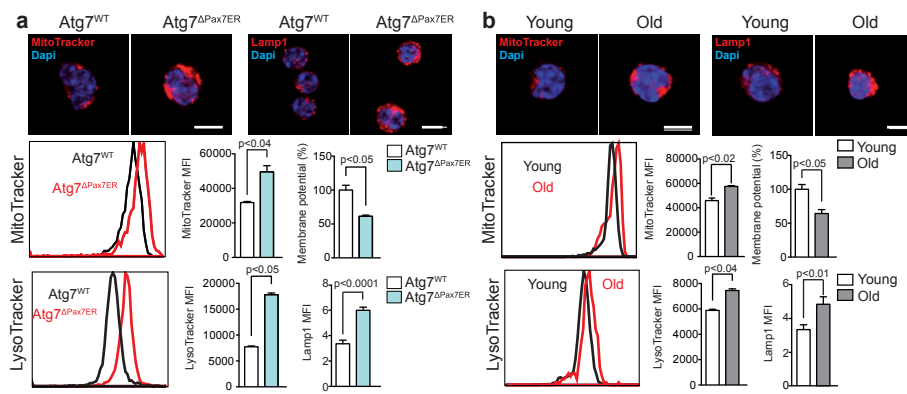


Figure 4

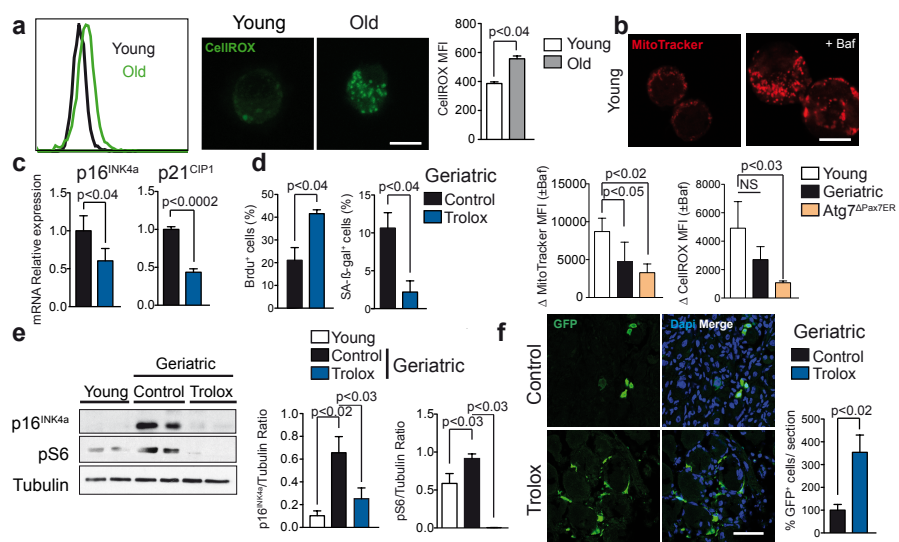


Figure 5



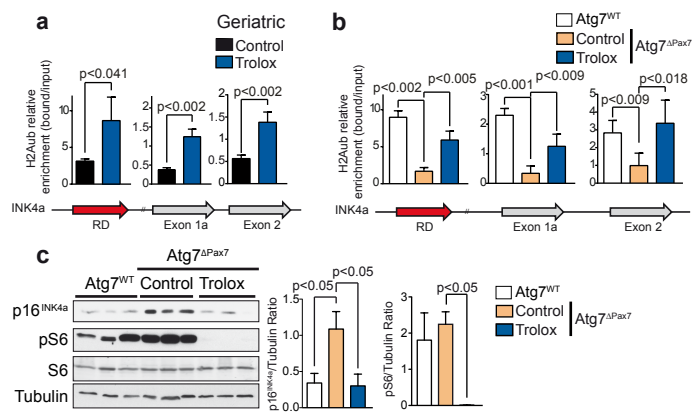
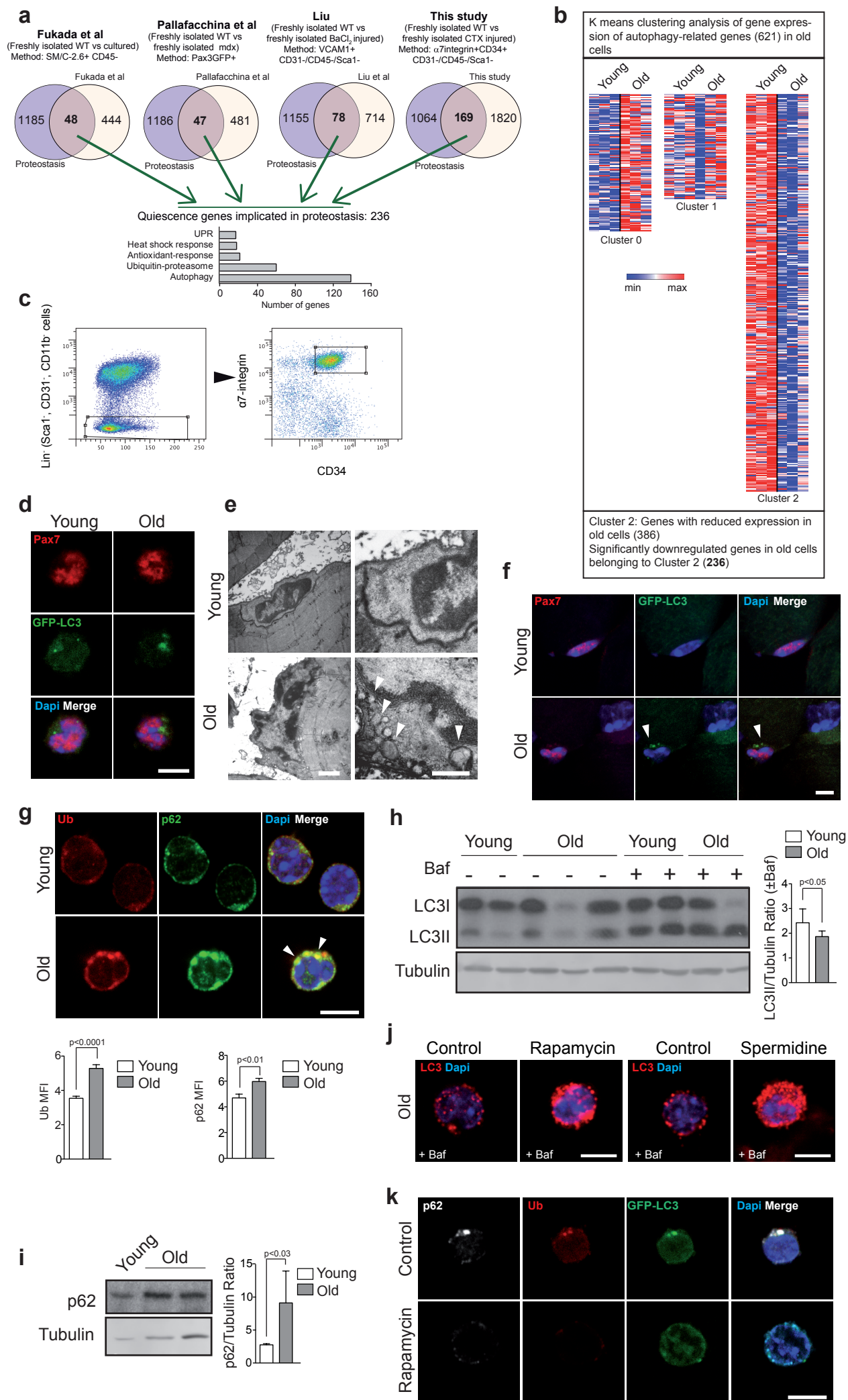
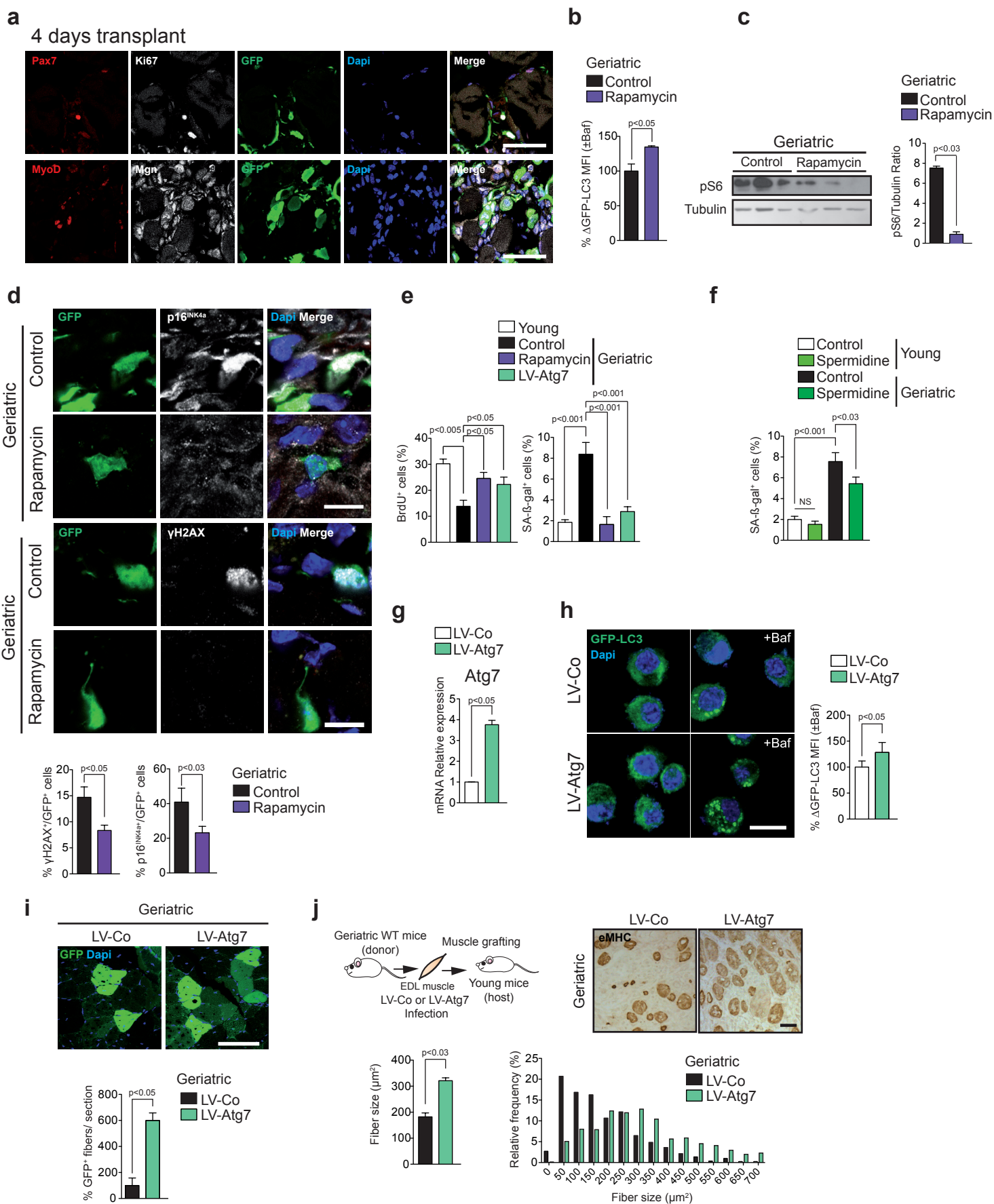
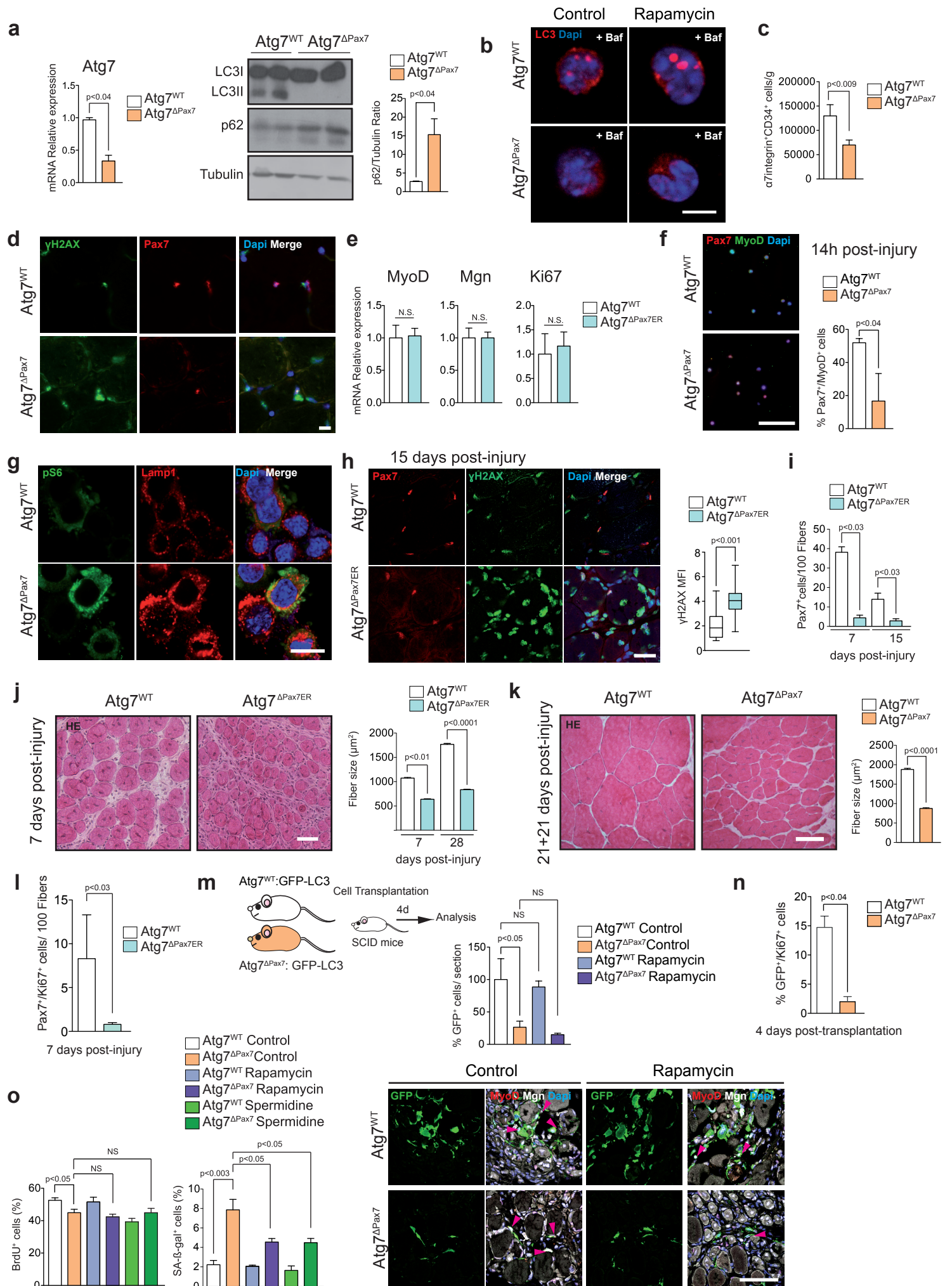


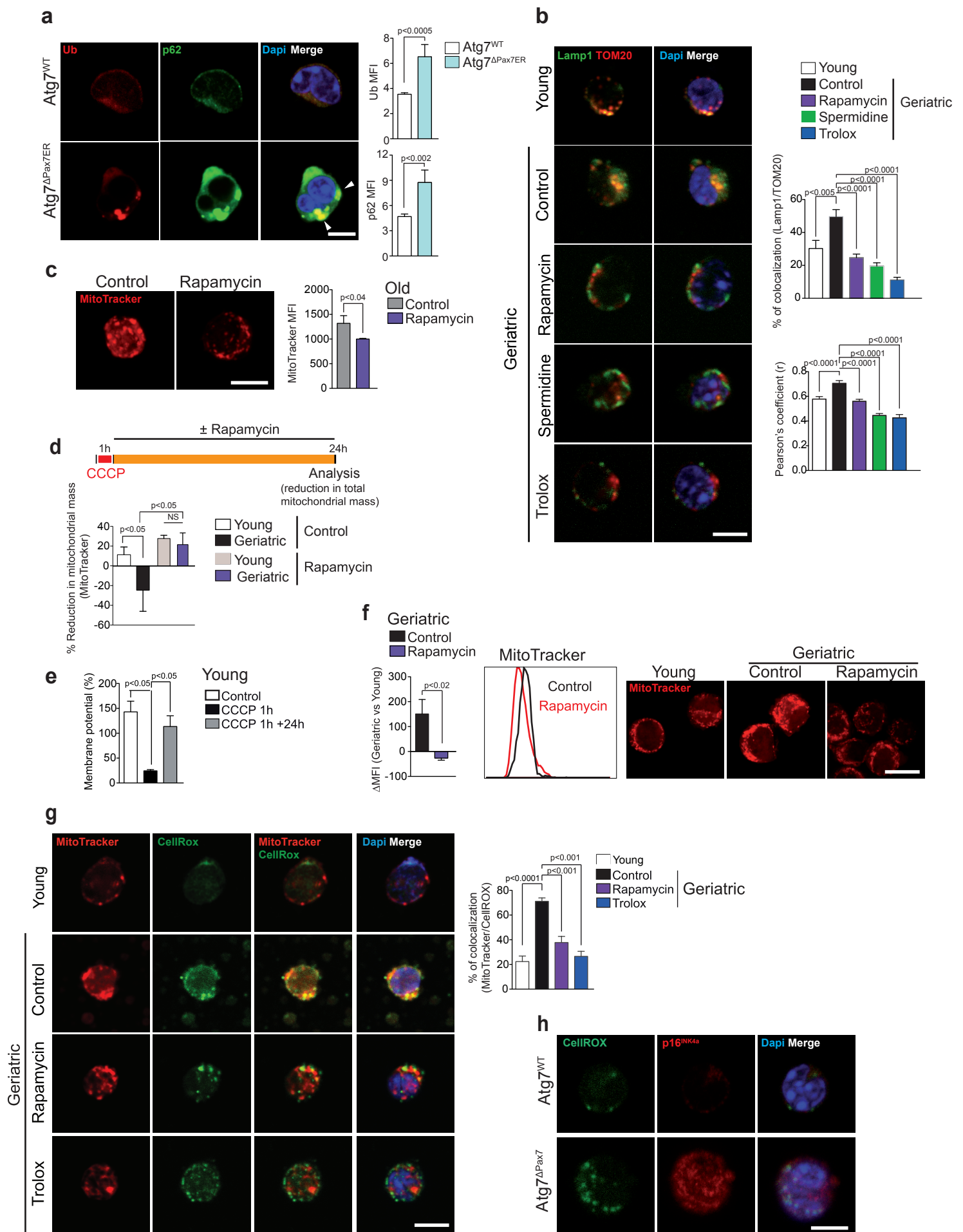
Figure 6

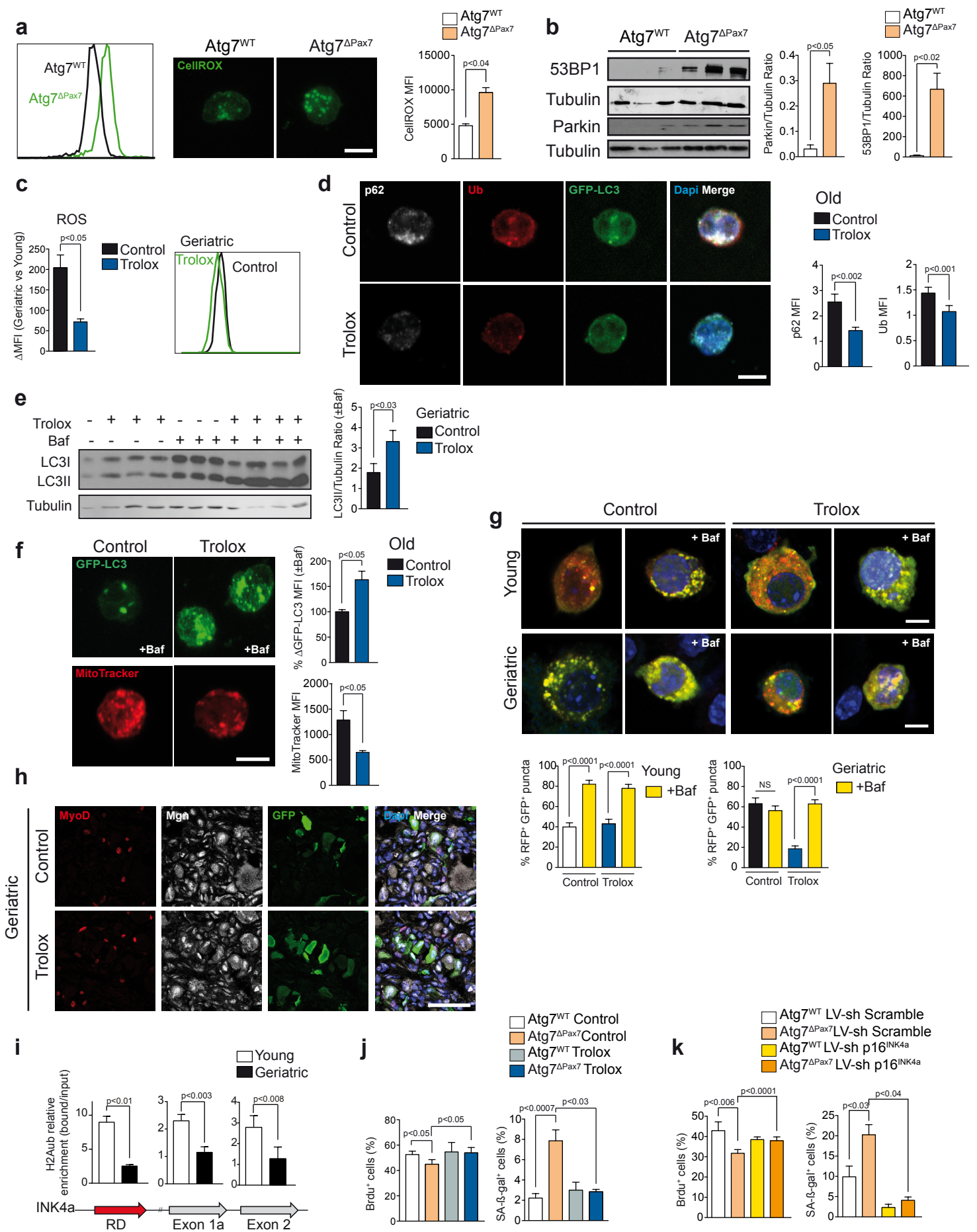


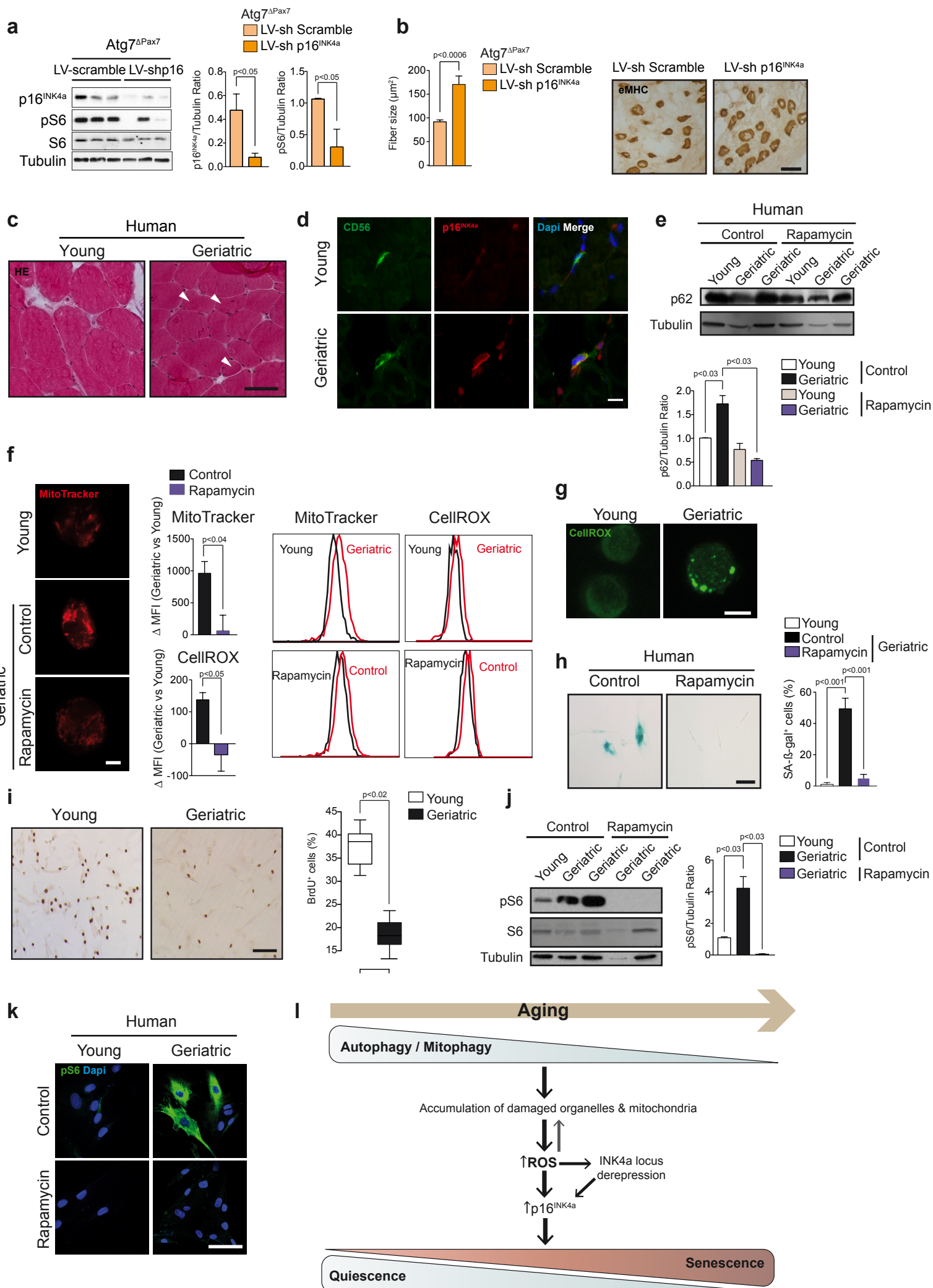






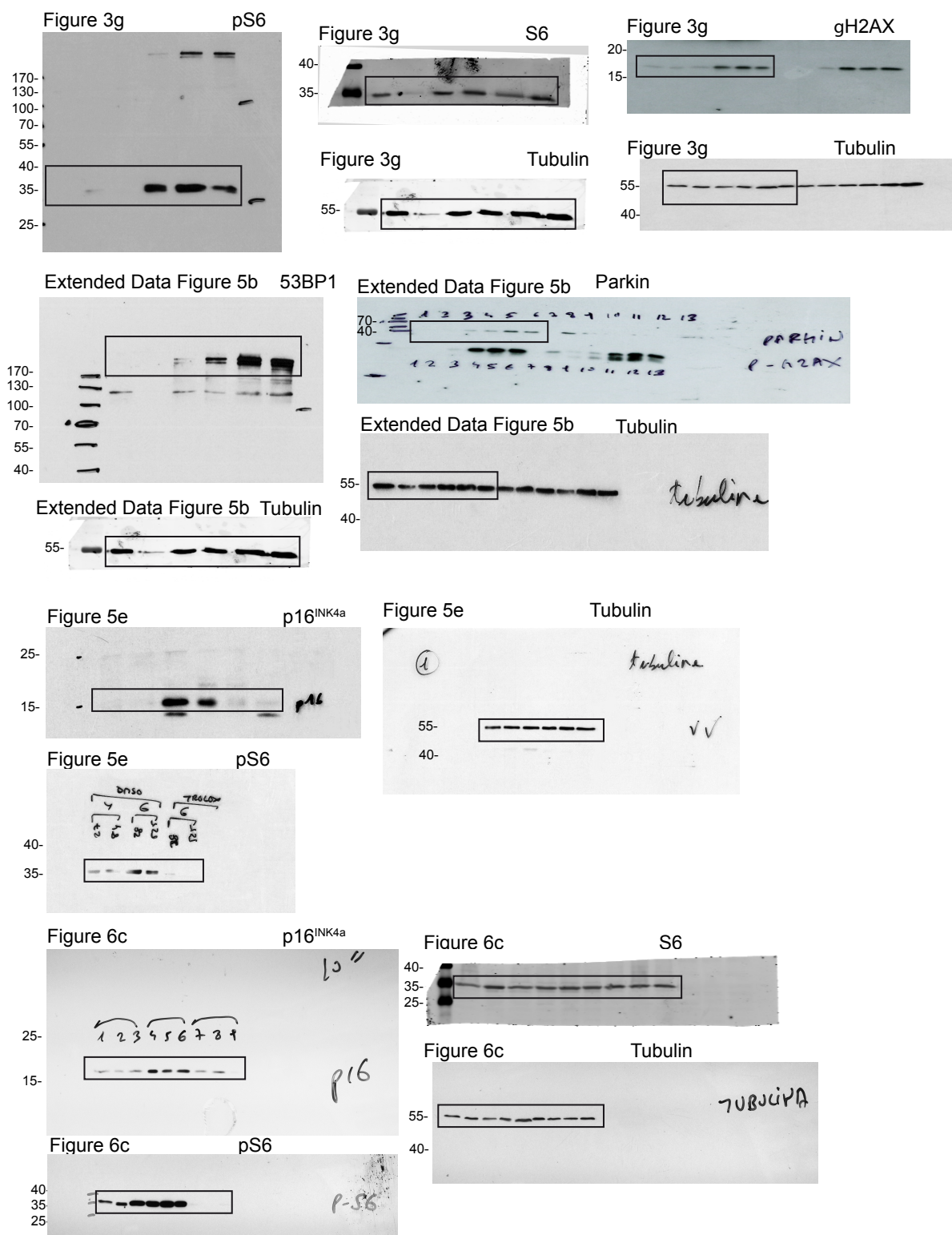








# Supplementary Figure - Uncropped scans with size marker indications





# Supplementary Figure - Uncropped scans with size marker indications

